JOURNAL OF GEOPHYSICAL RESEARCH, VOL. 106, NO. E3, PAGES 5057–5083, MARCH 25, 2001

Phyllosilicate-poor palagonitic dust from Mauna Kea Volcano (Hawaii): A mineralogical analogue for magnetic Martian dust?

R. V. Morris,[1] D. C. Golden,[2] D. W. Ming,[1] T. D. Shelfer,[3] L. C. Jørgensen,[4] J. F. Bell III,[5] T. G. Graff,[3] and S. A. Mertzman[6]

Abstract. The mineralogical and elemental composition of dust size fractions (<2 and <5 μm) of eight samples of phyllosilicate-poor palagonitic tephra from the upper slopes of Mauna Kea Volcano (Hawaii) were studied by X-ray diffraction (XRD), X-ray fluorescence (XRF), visible and near-IR reflectance spectroscopy, Mössbauer spectroscopy, magnetic properties methods, and transmission electron microscopy (TEM). The palagonitic dust samples are spectral analogues of Martian bright regions at visible and near-IR wavelengths. The crystalline phases in the palagonitic dust are, in variable proportions, plagioclase feldspar, Ti-containing magnetite, minor pyroxene, and trace hematite. No basal reflections resulting from crystalline phyllosilicates were detected in XRD data. Weak, broad XRD peaks corresponding to X-ray amorphous phases (allophane, nanophase ferric oxide (possibly ferrihydrite), and, for two samples, hisingerite) were detected as oxidative alteration products of the glass; residual unaltered glass was also present. Mössbauer spectroscopy showed that the iron-bearing phases are nanophase ferric oxide, magnetite/titanomagnetite, hematite, and minor glass and ferrous silicates. Direct observation by TEM showed that the crystalline and X-ray amorphous phases observed by XRD and Mössbauer are normally present together in composite particles and not normally present as discrete single-phase particles. Ti-bearing magnetite occurs predominantly as 5-150 nm particles embedded in noncrystalline matrix material and most likely formed by crystallization from silicate liquids under conditions of rapid cooling during eruption and deposition of glassy tephra and prior to palagonitization of glass. Rare spheroidal halloysite was observed in the two samples that also had XRD evidence for hisingerite. The saturation magnetization J_s and low-field magnetic susceptibility for bulk dust range from 0.19 to 0.68 Am^2/kg and $3.4x10^{-6}$ to $15.5x10^{-6}$ m^3/kg at 293 K, respectively. Simulation of the Mars Pathfinder Magnet Array (MA) experiment was performed on Mauna Kea Volcano in areas with phyllosilicate-poor palagonitic dust and with copies of the Pathfinder MA. On the basis of the magnetic properties of dust collected by all five MA magnets and the observation that the Pathfinder MAs collected dust on the four strongest magnets, the value for the saturation magnetization of Martian dust collected in the MA experiments is revised downward from 4±2 Am^2/kg to 2.5±1.5 Am^2/kg. The revised value corresponds to 2.7±1.6 wt % magnetite if the magnetic mineral is magnetite (using J_s = 92 Am^2/kg for pure magnetite, Fe_3O_4) or to 5.0±3.0 to 3.4±2.0 wt % maghemite if the magnetic mineral is pure maghemite (using J_s = 50 to 74 Am^2/kg for pure maghemite, γ-Fe_2O_3). Comparison of the magnetic properties of bulk Mauna Kea palagonitic dust to those for dust collected by MA magnets shows that the MA magnets extracted (culled) a subset (25-34 wt %) of composite magnetic particles from bulk dust. The extent of culling of Martian dust is not well constrained. Because the Mauna Kea palagonitic dust satisfies the essential constraints of the Pathfinder magnetic properties experiment (composite and magnetic particles capable of being collected by five MA magnets), a working hypothesis for the strongly magnetic mineral present in Martian dust and soil is magnetite (possibly Ti-bearing) formed by rapid crystallization from silicate liquids having volcanic and/or impact origins. Subsequent palagonitization of the glass produces the nanophase ferric oxide phases that dominate the spectral properties of Martian bright regions at visible and near-IR wavelengths. Magnetic and phyllosilicate-poor palagonitic dust from Mauna Kea Volcano is thus a spectral and magnetic analogue for magnetic Martian dust.

[1]NASA Johnson Space Center, Houston, Texas.
[2]Hernandez Engineering, Inc., Houston, Texas.
[3]Lockheed Martin Space Operations Company, Houston, Texas.
[4]Niels Bohr Institute for Astronomy, Physics and Geophysics, Ørsted Laboratory, University of Copenhagen, Copenhagen, Denmark.
[5]Department of Astronomy, Cornell University, Ithaca, New York.
[6]Department of Geosciences, Franklin and Marshall College, Lancaster, Pennsylvania.

Paper number 2000JE001328.
0148-0227/01/2000JE001328$09.00

1. Introduction

Palagonite is a yellow or orange mineraloid formed by hydration and devitrification of basaltic glass [e.g., *Bates and Jackson*, 1984]. Palagonitic materials are found throughout the world as subareal, subglacial, and submarine alteration products of basaltic glass that is produced by volcanic and, to a lesser extent, impact processes [*Morris et al.*, 2000, and references therein]. Palagonitic tephras from the upper slopes of Mauna Kea Volcano on the island of Hawaii have received widespread attention in planetary literature because certain ones are spectral analogues of the bright regions of the Martian surface at visible and near-IR wavelengths [e.g., *Singer*, 1982; *Morris et al.*, 1990, 1993, 2000; *Bell et al.*, 1993]. The analogue spectra are characterized by a generally featureless ferric absorption edge extending from ~400 to 750 nm and relatively constant reflectivity extending from 750 to beyond 2100 nm. As shown by reflectivity spectra, Mössbauer analysis, transmission electron microanalysis (TEM), X-ray diffraction (XRD), and selective dissolution studies, the pigment responsible for the ferric absorption edge is nanophase ferric oxide (np-Ox), which is nanometer-sized (<10 nm) ferric oxide particles with indistinct boundaries that are embedded in hydrated and poorly crystalline aluminosilicate matrix material [*Morris et al.*, 1993]. Martian bright regions have a similar spectral shape, but with subtle superimposed spectral features whose positions vary from place to place on the planet [e.g., *Murchie et al.*, 1993]. As shown by the spectral properties of mechanical mixtures of palagonitic tephra and well crystalline ferric oxide pigments [*Morris et al.*, 1997; *Morris and Golden*, 1998], these subtle features can result from subordinate amounts of different and crystalline ferric oxides (e.g., hematite or goethite) that are present in addition to np-Ox. The oxidized, ferric-rich Martian bright regions contrast with Martian dark regions, whose visible and near-IR spectra have significant contributions from ferrous iron, which is generally considered to be associated with pyroxene [e.g., *Mustard et al.*, 1997].

Previous Mössbauer studies of size separates of palagonitic tephra show that the doublet associated with np-Ox has the greatest relative area in the finest size fractions, implying that the products from alteration of the basaltic glass accumulate in the finest size fractions [*Morris et al.*, 1990, 1993, 2000; *Bell et al.*, 1993]. This result is supported by scanning electron microscopy (SEM) observations of coarse tephra particles which show friable palagonitic rinds [e.g., *Singer*, 1982; *Allen et al.*, 1981]; the rinds flake off and accumulate as fine-grained material. Small crystalline silicate and oxide phenocrysts (i.e., lithogenic minerals including feldspar, olivine, pyroxene, and titanomagnetite) that are completely or incompletely liberated from glass during its alteration will also accumulate in the fine fractions as discrete or composite particles, respectively, and possibly undergo alteration. TEM observations of small (5-1000 nm) lithogenic plagioclase and titanomagnetite grains embedded in palagonite are reported for palagonitic tephra PN-9 [*Morris et al.*, 1993]. Petrographic studies show that larger phenocrysts (1-10 μm) of these minerals are also present [*Morris et al.*, 1990]. We have suggested that spectral-analogue palagonitic tephra may also be a magnetic analogue of Martian surface materials because the strongly magnetic titanomagnetite makes the tephra somewhat magnetic [*Morris et al.*, 1990, 2000]. The hydrated aluminosilicate matrix remaining after precipitation of np-Ox particles can be X-ray amorphous [*Morris et al.*, 1990, 1993, 2000] or may be partially replaced by phyllosilicates and zeolites [*Golden et al.*, 1993].

Dust-specific Martian data include the results of the Viking and Pathfinder magnetic properties experiments, extended visible multispectral data (440-1000 nm) from the Imager for Mars Pathfinder (IMP) experiment, and dust opacities [e.g., *Hargraves et al.*, 1979, 2000; *Hviid et al.*, 1997, 2000; *Madsen et al.*, 1999; *Markiewicz et al.*, 1999]. There is general agreement that a strongly magnetic mineral is present in the dust, but there is not agreement on its mineralogy or mode of formation. The preferred interpretation of *Hargraves et al.* [1977, 1979, 2000], *Hviid et al.* [1997], and *Madsen et al.* [1999] is that maghemite (γ-Fe_2O_3) is the strongly magnetic component in Martian dust (and soil) and that it is present as a cementing agent formed as a result of hydrolytic alteration of basaltic materials, producing a dust predominantly composed of composite particles containing variable proportions of maghemite. These authors acknowledge, but do not prefer, explanations involving lithogenic magnetic phases (e.g., magnetite/titanomagnetite and/or their oxidation products) as suggested by others [*Coey et al.*, 1990; *Morris et al.*, 1990, 2000].

The clay (<2 μm) and clay plus fine silt (<5 μm) size fractions, which are routinely obtained during studies of terrestrial soils to characterize products of alteration and weathering, are size analogues for aeolian dust on Mars. An average particle diameter of 3.4 ± 0.6 μm is reported by *Markiewicz et al.* [1999] for measurements during the Mars Pathfinder mission. Other estimates for the mean particle diameter of Martian dust range from 0.2 to 10 μm [e.g., *Murphy et al.*, 1993; *Pollack et al.*, 1995].

Mineralogical analyses of the "dust" size fractions (<2 μm and <5 μm) of spectral-analogue palagonitic tephra are important for understanding the mineralogical composition and formation process for Martian dust. Is the dust primarily an alteration product of basaltic glass (i.e., palagonite) in which crystalline mineral phases are inherited? Have inherited phases altered, e.g., magnetite oxidation to maghemite? Are crystalline mineral phases formed as alteration products? Are the magnetic properties of Martian dust consistent with palagonite-style alteration processes? These questions pertain not only to the mineralogical identification of the magnetic phase but also to its concentration and distribution within discrete dust particles. We report chemical and mineralogical data for eight samples of palagonitic dust that are the <2 μm or <5 μm size fraction of material that was separated from bulk samples of palagonitic tephra (usually the <1 mm size fraction) which came from various locations on the upper slopes (2010-3730 m) of Mauna Kea Volcano (Hawaii). Two palagonitic dust samples were heated in air to ~495°C to study thermal effects, and two were magnetically separated. As previously reported [*Morris et al.*, 1990, 1993, 2000], the unheated tephras considered in this paper are spectral analogues for Martian bright regions at visible and near-IR wavelengths, do not have detectable phyllosilicates based on XRD powder patterns, and have Fe-Ti oxides as a strongly magnetic mineral. We extend the previous work with new data (1) to identify and characterize the mineralogical composition of component phases, (2) to determine the distribution of iron among these phases, (3) to determine if individual phases occur as discrete particles or as components in composite particles, and (4) to determine the chemical and

Table 1. Collection Sites on Mauna Kea Volcano and References to Previous Work for Palagonitic Tephra Used to Obtain Palagonitic "Dust"

Tephra	Collection Site (Elevation)	References[a]
HWHP301	gully north of Visitor's Center (2830 m)	1
HWMK1	gully near Visitor's Center (2830 m)	1,2
HWMK530	Puu Kilohana cinder cone (2890 m)	1,3
HWMK600 and HWMK612	south side of road to Very Long Baseline Array telescope (3730 m)	1
HWMK919	north side of road to Very Long Baseline Array telescope (3730 m)	4
JSC Mars-1	Puu Nene cinder cone (2010 m)	1,5
PN-9	Puu Nene cinder cone (2010 m)	1,6

[a]References: 1, *Morris et al.* [2000]; 2, *Morris et al.* [1990]; 3, *Morris et al.* [1997]; 4, this study; 5, *Allen et al.* [1998]; 6, *Morris et al.* [1993].

structural purity and size distribution of magnetic oxide particles. Analytical techniques included reflectance spectroscopy (350-2100 nm), Mössbauer spectroscopy, magnetic properties, XRD, and TEM.

We also report results of magnetic properties experiments done on Mauna Kea Volcano using replicas of the Pathfinder Magnet Array in the same places where the samples discussed above were collected. We documented the collection of aeolian palagonitic dust as a function of time by digital photography and analyzed the dust collected by individual array magnets by magnetic properties methods and Mössbauer spectroscopy. These experiments provide calibration data for the Magnet Array and constrain the origin, mode of occurrence, and mineralogical composition of the strongly magnetic phase in Martian dust.

2. Samples and Methods

2.1. Samples

Samples of palagonitic tephra (Table 1) were collected at elevations between ~2010 and 3730 m on Mauna Kea Volcano (Hawaii); the average rainfall is 50-75 cm/yr [*Brady et al.*, 1999]. All samples except JSC Mars-1 were collected in the field as the <1 mm size fraction using a wire mesh sieve. The collection of JSC Mars-1 is described by *Allen et al.* [1998]. The clay (<2 μm) or clay plus fine silt (<5 μm) size fractions were normally obtained from <1 mm size fractions by ultrasonic dispersement and sedimentation (both in H_2O at pH = 9) using a density of 2.65 g/cm^3 to calculate settling times [*Jackson,* 1985]. Sonication also disrupts the fragile weathered portions of the tephra, concentrating them into the <2 or <5 μm size fraction. After sedimentation the dust size fractions were washed by dialysis with neutral H_2O, flocculated, and freeze dried. Because <1 mm tephra was no longer available, the <90 and 45-90 μm size fractions (obtained by mechanical sieving) were used as the source material for the <2 μm size fraction of HWMK1 and PN-9, respectively. The gravimetric distributions of size fractions are summarized in Table 2. Splits of the <2 μm size fraction of HWHP301 and HWMK600 (batch B) were heated in platinum crucibles in air at 495±10°C for 12-14 hours to study thermal effects.

Splits of the <5 μm size fractions of HWHP301 and HWMK919 were magnetically fractionated by repeatedly placing a plastic-coated hand magnet in a dust-ethanol suspension produced by ultrasonic agitation. Material adhering to the magnet was collected as the magnetic <5 μm fraction, with the residue as the nonmagnetic <5 μm fraction. After removal of excess ethanol by centrifugation, the magnetic separates were air dried for 24 hours.

To estimate spectral and XRD detection limits of smectite in phyllosilicate-poor palagonitic tephra, we prepared mixtures of powders of palagonite (HWMK600) and smectite (SWa-1; a smectite from Washington state that was obtained from Source Clay Minerals Repository of the Clay Minerals Society). Powders were prepared by mechanical grinding of

Table 2. Particle-Size Distribution of Palagonitic Soils Dispersed by Sonication in Aqueous Suspension

	Initial Size	Mass in Size Fraction, wt %						
Sample	Fraction[a]	<2 μm	2-5 μm	<5 μm	5-53 μm	53-500 μm	500-1000 μm	5-1000 μm
HWMK1	<90 μm	10.02	4.04		76.04	9.89	0.00	
HWHP301	<1 mm	4.47	7.93		49.34	26.53	11.72	
HWMK530	<1 mm	1.90	4.27		20.43	49.21	24.18	
HWMK600[b]	<1 mm	1.26	0.19		16.01	56.22	26.33	
HWMK612	<1 mm	2.55	4.73		36.65	47.71	8.36	
HWMK919	<1 mm			15.3				84.7
JSC Mars-1	<1 mm	0.46	0.56		4.53	75.72	18.73	
PN-9	45-90 μm	3.21	1.98		66.22	28.59	0.00	

[a]For the six samples whose parent size fraction is <1 mm, the average mass in the <5 μm size fraction is 7.3±5.2%.

[b]The <2 μm fraction of HWMK600 was obtained in two separation procedures [Morris et al., 2000]. Batch A was obtained using unprocessed <1 mm palagonitic tephra. Batch B was separated from the 2-1000 μm residual of batch A after additional sonication. The size distribution refers to batch A.

the palagonite (<1 mm size fraction) and smectite (1-4 cm pieces) until they passed a 90 μm sieve. The powders were combined in known proportions (0, 1.1, 2.8, 5.0, 10.1, 17.8, 49.8, and 100 wt % smectite) and blended ultrasonically in ethanol. Mixtures were air dried for 24 hr.

2.2. Instrumental Methods

A Scintag XDS2000 X-ray diffractometer using Cu(Kα) radiation was employed to obtain powder XRD patterns. The goniometer was aligned against the peaks for silicon powder, and the instrumental sensitivity calibrated against the silicon peak at 28.442° 2θ. Powder patterns between 2° and 15° 2θ, which is where the basal diffraction peaks for smectite and other phyllosilicates occur (e.g., smectite ~1.5 nm, chlorite ~1.4 nm, mica ~1.0 nm, and halloysite ~1.0 and ~0.7 nm), were collected at a scan speed of 0.25° 2θ/min and a step size of 0.02 °2θ; full scans (5° to 70° 2θ) were collected at 0.5° 2θ/min scan speed and 0.02° 2θ step size. Powder XRD patterns were obtained on unoriented mounts for all samples and on magnesium-saturated oriented mounts with and without glycerol solvation for selected samples. The reference database for XRD powder spectra was the Powder Diffraction File Release 1998 issued by the International Centre for Diffraction Data.

TEM analyses were done with a JEOL 2000FX scanning transmission electron microscope operated at 160 or 200 kV, and chemical analyses were done with a built-in Link eXL energy dispersive X-ray analysis system. For TEM analysis, clumps of freeze-dried palagonitic dust were embedded in EMBED-812 epoxy and cut in ~70 nm sections using a diamond knife. The sections were mounted on a carbon-coated Formvar substrate on a Cu grid for TEM observation. A Cary-14 spectrophotometer configured with an integrating sphere (23 cm diameter) was used to obtain visible and near-IR diffuse reflectance spectra (350-2100 nm) at room temperature. The interior of the integrating sphere and the reflectivity standard were Halon, whose optical properties are described by *Weidner and Hsia* [1981]. Transmission Mössbauer spectra were obtained at room temperature with Ranger MS-1200 Mössbauer spectrometers. Mössbauer absorbers were prepared by uniformly dispersing ~50 mg/cm^2 of sample (~5 mg/cm^2 of natural Fe) in epoxy. The Mössbauer source and its intensity were ^{57}Co(Rh) and ~20 mCi, respectively. Mirror image spectra (1024 channels) were obtained using a triangular waveform and folded to a single spectrum using velocity data obtained with a laser interferometer. Folded spectra were fit with an in-house computer program (JSCFIT). Magnetic properties were measured on a PAR Model 151 Vibrating Sample Magnetometer and a Bartington Model B2 susceptibility meter. Major element chemistry was determined by X-ray fluorescence (XRF) using a 9:1 $Li_2B_4O_7$-sample flux-fusion procedure to prepare glass disks and a Philips 2404 XRF spectrometer equipped with a 4 kW Rh X-ray tube [see *Boyd and Mertzman*, 1987]. Loss on ignition (LOI) was ascertained by heating an exact aliquot of sample powder at 950°C in air for a minimum of 1 hour. Because major element analyses were done on the residue of LOI measurements, total iron is reported as Fe_2O_3T. The Fe^{2+} concentration was measured on unheated samples using a modified *Reichen and Fahey* [1962] procedure. See *Morris et al.* [2000] for a more complete description of instruments and procedures.

2.3. Magnet Array Experiments

The Magnet Arrays (MA) flown by Mars Pathfinder are described by *Smith et al.* [1997], *Hviid et al.* [1997], *Gunnlaugsson et al.* [1998], and *Madsen et al.* [1999]. Briefly, each array consists of two subarrays, one with two permanent magnets whose strengths are comparable to the magnets flown on the Viking landers and the other with three weaker magnets. The five magnets are embedded in magnesium metal and their relative strengths (B|∇B|) are 100:9:3:0.7:0.2. Each magnet is a cylindrical magnet with a concentric ring magnet ("target" pattern), and they are arranged in order of decreasing strength from right to left. The flat surface of each subarray makes a +30° angle with the horizontal. The magnesium metal surfaces were roughened by glass-bead blasting and then coated with a layer (0.5 μm thick) of platinum metal. The scale length for the roughness is ~10 μm [*Madsen et al.*, 1999], which is larger than the diameter of dust particles.

The two Magnet Arrays used in our experiments are magnetically equivalent to, but slightly different in their method of fabrication from, the ones flown on Mars Pathfinder (M. B. Madsen, personal communication, 2001). The MA used by *Morris et al.* [1998a] for laboratory experiments and for the 1998 Mauna Kea experiments (HWMK8MA00 and -01) has a hard clear lacquer finish instead of a platinum coating, and the two subarrays were mounted to a flat plastic base with a +30° angle between array surfaces and base plate. The MA used for the 1999 Mauna Kea experiments (HWMK9MA05-08, -16, -19, -23 through -25) was fabricated from aluminum instead of magesium metal, and the aluminum surface was anodized after glass-bead blasting. The two subarrays were mounted to a flat aluminum metal base with a +30° angle between array surfaces and base plate. For dust-sized particles the different MA surface finishes and the difference in gravity between the Earth and Mars are not considered important differences affecting MA performance because, for dust loadings similar to those that prevailed on Mars, dust patterns on the magnets were reproduced in inverted orientation in laboratory experiments (M. B. Madsen, personal communication, 2001). The Magnet Arrays used in our experiments (and those flown on Mars Pathfinder) were made at the Ørsted Laboratory, Niels Bohr Institute for Astronomy, Physics, and Geophysics, University of Copenhagen, Denmark, and were provided courtesy of Jens Martin Knudsen and Morten Bo Madsen.

MA experiments were done on Mauna Kea Volcano in September of 1998 and August of 1999 by placing arrays on the ground or on a small rock and waiting for dust to collect. We found that the ambient environment was not sufficiently dusty to complete experiments in a timely manner. Therefore dust was artificially produced by mechanical agitation of palagonitic soil ~1 m upwind from the MA. The usual procedure was to allow palagonitic soil to drop from a height of ~0.5 m, allowing the finer particles to be entrained in the wind and blown over the array. The MA was usually oriented so that wind impinged on the front, but some experiments were done with the wind impinging on the back and sides. The wind direction was relatively constant, but the speed was variable. Dust was collected from the base plate and from the target patterns developed on individual magnets by using a small paint brush to carefully sweep the material off onto glassine paper before transferring it to plastic vials. For many

experiments, it was not possible to collect enough dust for subsequent analysis from magnet 4 and especially magnet 5, the weakest magnet. For all magnets, there was a tendency for collected dust to blow away when removed from the attractive force of the magnets, despite our best efforts to shield the MA from wind gusts during this operation. We did not retain sample from a magnet when some portion was observed to blow away during transfer to sample vials. It was necessary to combine samples from several experiments run under nominally the same conditions to have enough material to analyze in the laboratory. Dust collected from base plates was used as a sample representative of the bulk dust presented to MA surfaces.

The environmental conditions during our MA experiments are only approximately known. As measured at the UKIRT Weather Station on the summit of Mauna Kea (http://www.ukirt.jach.hawaii.edu), the air temperature, dew point, relative humidity, and barometric pressure were 277-282 K, 253-275 K, 36-70%, and 61.5-62.0 kPa (615-620 mBar), respectively. All experiments were done in bright sunlight. The wind speed was not measured in 1998 but was measured in 1999 using a wind speed indicator (Davis Instruments). The advantages of conducting MA experiments on Mauna Kea include an unlimited supply of palagonitic dust and the availability of low absolute humidity and bright sunlight, both of which promote dispersal of dust particles. Our qualitative observation is that dispersal was not as effective (smaller dust cloud that settled out more quickly) when conditions were cloudy and the humidity was higher.

3. Mineralogy of Palagonitic Dust

3.1. Major Element Chemistry

The major element chemistry for the parent tephra (<1 mm size fractions) of our dust samples is published by *Morris et al.* [2000], except for sample HWMK919. The major element chemistry of the <1 mm and <5 μm size fractions of HWMK919 is given in Table 3 along with corresponding data for the average composition of unaltered tephra [*Morris et al.*, 2000]. Using data from this study and *Morris et al.* [2000], we also calculated the average composition of the <1 mm size fraction of phyllosilicate-poor palagonitic tephra (14 samples) and the average composition of derived palagonitic dust (3 samples). As discussed by *Morris et al.* [2000], the difference in chemistry between unaltered tephra and palagonitic tephra results from oxidative hydrolytic alteration at ambient temperatures in which the palagonitic material is the solid residue of aqueous leaching. The dust contains the highest proportion of alteration products. Relative to unaltered materials, the palagonitic dust is highly oxidized, enriched in TiO_2, Al_2O_3, Fe_2O_3T, MnO, and P_2O_5, and depleted in SiO_2, MgO, CaO, K_2O, and Na_2O. The enrichments are passive, resulting from the removal of the other elements by leaching.

3.2. Powder X-Ray Diffraction

The variation in intensity of the basal reflection for smectite at 1.51 nm for random powder mounts of mixtures between smectite (SWa-1) and palagonite (HWMK600) is shown in Figure 1. The palagonite itself has no detectable peaks that can be attributed to smectite or any other phyllosilicate. The peak at 0.645 nm results from plagioclase feldspar. The smectite peak is just visible and clearly present at 1.1 and 2.8 wt % smectite, respectively, implying that the smectite detection limit is ~1-3 wt %. The intensity of the smectite peak increases (and the plagioclase peak decreases) with increasing smectite concentration. Note that the detection limit is with respect to SWa-1 and under conditions that no special procedures were used to concentrate phyllosilicates from bulk samples. The usual procedure for analysis of natural (unground) soils is to do XRD analyses on oriented mounts after cation saturation and solvation of the <2 μm size fraction where the fine-grained weathering products (like phyllosilicates) are preferentially concentrated.

XRD powder patterns for unoriented mounts of fine powders of the <1 mm size fraction and for the <2 or <5 μm size fraction are shown in Figure 2 for each palagonitic tephra. No peaks corresponding to the basal reflections of smectite (1.51 nm) or any other phyllosilicate were detected, implying that <1-3 wt % smectite is present in each sample. If we assume that phyllosilicates, if present, are entirely concentrated in the <2 μm size fraction, the upper limit for the smectite content of the <1 mm size fraction is about 0.1-0.3 wt %, assuming a percentage mass of 10 wt % for the <2 μm size fraction (Table 2). Smectite peaks are also not observed in Mg-saturated oriented mounts (with and without glycerol solvation). Because the intensities of the basal reflections are enhanced in oriented mounts and because the largest percentage mass for the <2 μm size fraction (10 wt %) was used for the calculations, 0.1-0.3 wt % is a conservative upper limit for the smectite concentration. The XRD powder patterns of the clay fraction of two oriented samples (HWMK600 and HWMK612) show a very weak peak near 1.41 nm, which we tentatively attribute to hydroxy interlayered vermiculite (HIV) or chlorite. Aeolian mica and quartz from China are sometimes reported in Hawaiian samples [e.g., *Syers et al.*, 1969], and the HIV may be an alteration product of the mica.

If the dust size fraction has no detectable crystalline phyllosilicates, what is its XRD mineralogy? To answer this question, XRD data were obtained over the range 15°-70° 2θ. The XRD spectra in Figure 3 are arranged in order of decreasing saturation magnetization (Table 4). As expected, because magnetite is a strongly magnetic mineral (J_s ~ 92 Am^2/kg [e.g., *Morris et al.*, 1985]), the intensity of the 0.252 peak (the most intense peak in the magnetite spectrum) decreases in the same order. The peaks at 0.297, 0.161, and 0.148 nm, which are clearly evident in the spectra with the most intense 0.252 nm peak (HWHP301 and HWMK612), are also magnetite peaks. These peaks are not evident in the samples with the least intense 0.252 nm peaks (PN-9 and JSC Mars-1), presumably because their intensities are too low.

In Figure 4 we compare XRD data for HWHP301 (<2 μm) near 35° 2θ and between 55° and 65° 2θ to corresponding data for a natural magnetite (MTISH1) and a natural maghemite (MCIS1), which are described by *Morris et al.* [2000]. The vertical dashed lines locate peak maxima for the <2 μm size fraction of HWHP301. The HWHP301 positions correspond closely to those for MTISH1, showing that the spinel phase is a magnetite and not a maghemite. This comparison does not exclude the presence of substitutional impurities in the magnetite. A significant amount of Ti can be accommodated in the structure without significantly shifting the position of the magnetite lines. As discussed below, TEM data show that the magnetite contains Ti. The greater width of the magnetite lines in the tephra compared to MTISH1

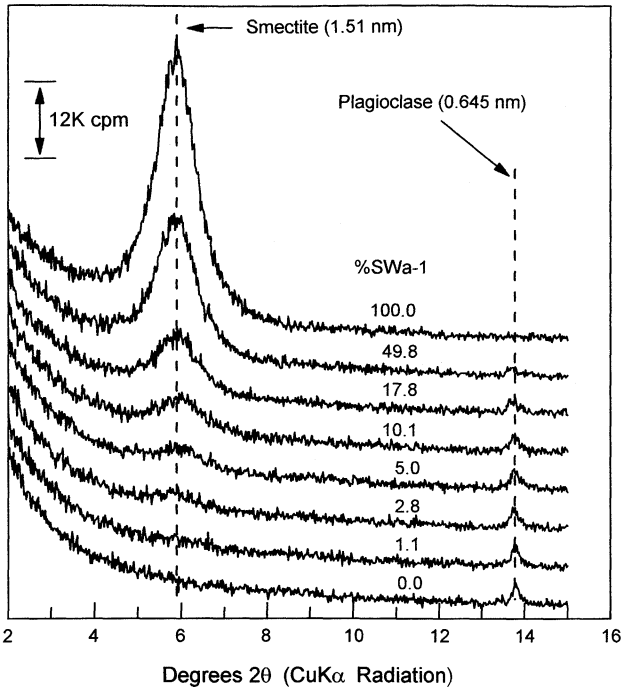

Figure 1. XRD powder patterns (unoriented) for mixtures of fine powders of HWMK600 and smectite SWa-1. The basal diffraction peak (1.51 nm) becomes visible by 2.8 wt % smectite. CPM, counts per minute.

implies small particles, poor crystallinity, and/or variable composition. Figure 4 also shows that heating HWHP301 in air at 495°C results in the shift of magnetite XRD lines to higher °2θ to positions corresponding to maghemite.

In addition to magnetite, all <2 and <5 μm size fractions contain plagioclase feldspar. The peak at 0.321 nm is the most intense peak in the spectrum of plagioclase feldspar, and the sharp peaks between 22° and 28° 2θ that are present in the samples with a strong 0.321 peak are also plagioclase peaks (Figure 3). The intensities of plagioclase and magnetite peaks do not correlate. Dust samples that have the most intense plagioclase peaks (HWMK530 and HWMK600 (batches A and B)) have intermediate magnetite peak intensities. Plagioclase feldspar is the major XRD phase in bulk (<1 mm) tephra samples [*Morris et al.*, 2000]. The two sharp peaks at 0.299 and 0.295 nm result from pyroxene, and their intensities seem to correlate with the magnetite 0.252 nm peak. However, this happens because there is a magnetite peak at 0.297 nm. The weak peak at 0.269 nm, which is present in all samples except PN-9 and JSC Mars-1, can be assigned to the most intense peak in the hematite spectrum.

Broad XRD peaks with poorly defined positions are present near 0.34, 0.23, and 0.15 nm in most samples (Figure 3), indicating the presence of X-ray amorphous phases (Figure 3). By "X-ray amorphous" we mean phases that are characterized by short-range structural order and have one or more broad (>2 °2θ) powder X-ray diffraction peaks. These three broad peaks are most apparent in samples where contributions from more crystalline phases (particularly feldspar) are the weakest (e.g., HWHP301, HWMK612, HWMK1, PN-9, and JSC Mars-1). The broad peak centered near 0.34 nm is the most intense, and it and the weaker peaks near 0.23 and 0.15 nm can be assigned to allophane ($Al_2O_3 \cdot 2SiO_2 \cdot nH_2O$) [e.g., *Henmi et al.*, 1981; *Moro et al.*, 2000] and residual basaltic glass which has a broad peak in the 0.35-0.30 nm region [e.g., *Palmer et al.*, 1988]. The broad peak near 0.15 nm is also consistent with the presence of

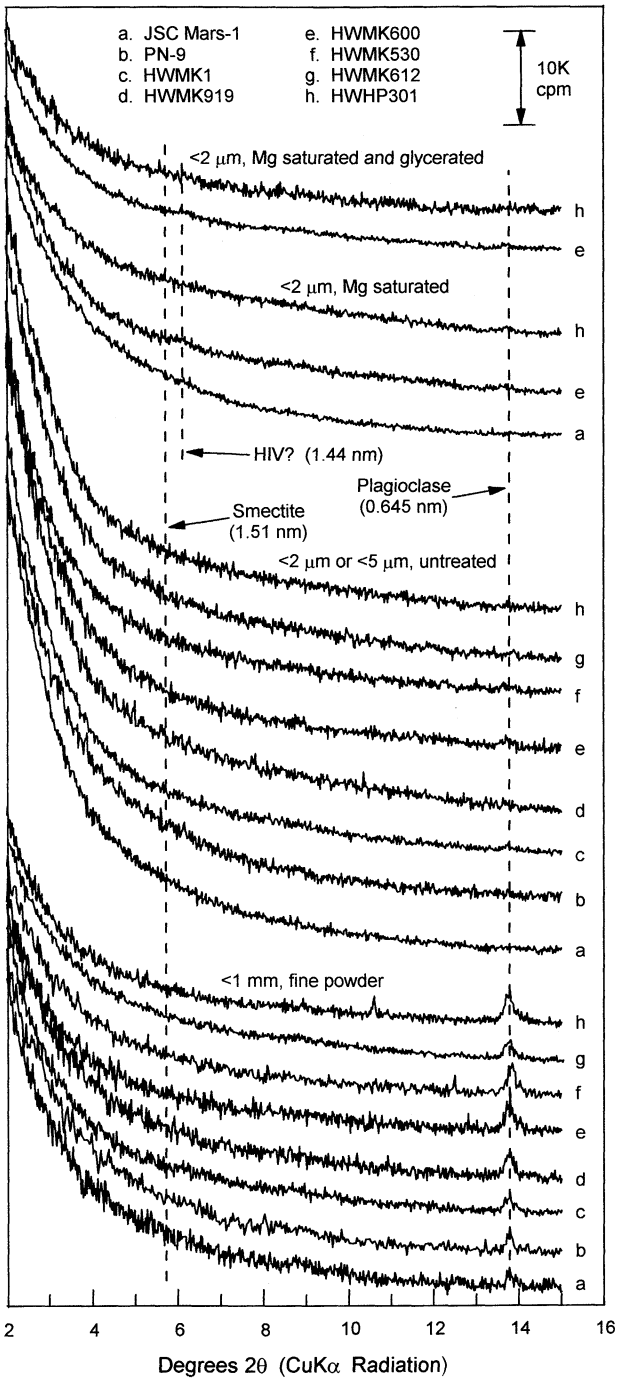

Figure 2. XRD powder patterns (2°-15° 2θ) of random powder mounts of finely ground bulk (<1 mm) palagonitic tephra, unoriented mounts of dust size fractions (<2 or <5 μm), and oriented mounts (Mg saturated and Mg saturated and glycerated) of selected palagonitic dust samples. Well crystalline phyllosilicates are not detected in bulk soil and dust size fractions because of the absence of a basal diffraction peak (e.g., no 1.51 nm smectite peak). The peak at 0.645 nm results from plagioclase feldspar, which is abundant in the bulk but not the dust size fractions. HIV, hydroxy interlayered vermiculite; CPM, counts per minute.

Table 3. Major Element Compositions of <1 mm Palagonitic Tephra and Palagonitic Dust

	HWMK905,[a] <1 mm	HWMK919,[b] <1 mm	HWMK919, <5 μm	HWMK923,[c] <1 mm	Average Unaltered Hawaiitic Tephra (6 Samples)[d]		Average <1 mm Palagonitic Tephra (14 Samples)[d,e]		Average Palagonitic Dust (3 Samples)[d,e]	
					Average	SD[f]	Average	SD	Average	SD
SiO_2	47.28	42.76	31.46	48.56	49.21	1.85	44.93	2.83	31.03	0.73
TiO_2	2.94	3.52	5.30	2.74	2.94	0.56	3.30	0.50	5.39	0.16
Al_2O_3	17.82	23.95	33.63	18.32	17.20	0.67	20.76	1.86	34.60	2.00
Fe_2O_3T	13.80	15.49	22.33	12.39	12.58	2.23	14.75	1.65	20.94	1.23
MnO	0.25	0.31	0.46	0.23	0.21	0.01	0.26	0.03	0.45	0.09
MgO	4.90	3.36	1.28	4.34	4.00	0.39	4.66	1.11	1.52	0.21
CaO	6.16	4.72	1.67	6.16	6.55	0.34	5.86	0.39	1.98	0.52
Na_2O	3.91	2.97	1.11	4.28	4.24	0.26	3.27	0.73	1.15	0.37
K_2O	1.33	0.89	0.22	1.62	1.87	0.09	1.07	0.41	0.30	0.13
P_2O_5	0.93	1.23	2.25	0.89	0.84	0.04	0.90	0.11	2.45	0.17
V, μg/g	145	135	152	130	137	44	153	34	211	65
Cr, μg/g	101	132	126	77	23	16	116	76	82	39
Total	99.32	99.20	99.71	99.53	99.64	0.23	99.77	0.15	99.82	0.10
LOI[g]	4.86	12.67	19.69	3.27	1.48	0.47	9.28	5.41	24.39	5.73
FeO	5.35	2.75	0.19	3.39	6.49	1.42	4.60	1.14	2.43	2.18
Fe_2O_3	7.85	12.43	22.12	8.62	5.37	0.88	9.64	1.65	18.23	3.47
Fe^{3+}/Fe^{2+}	1.32	4.07	105	2.29	0.74	0.14	2.04	0.86	37.9	57.9

[a]Collected south flank of Puu Kilohana cinder cone. Reference tephra for MA experiments HWMK9MA05 through HWMK9MA08 and HWMK9MA16.
[b]Collected north side of road to Very Long Baseline Array telescope. Reference tephra for MA experiments HWMK8MA00, HWMK8MA01, and HWMK9MA19.
[c]Collected south side of road to Very Long Baseline Array telescope. Reference tephra for MA experiments HWMK9MA23 through HWMK9MA25.
[d]*Morris et al.* [2000].
[e]This study.
[f]Standard deviation.
[g]Loss on ignition.

2-XRD-line ferrihydrite ($5Fe_2O_3 \cdot 9H_2O$) and/or a phase referred to as nanophase hematite [*Morris et al.*, 1991] (or, collectively, nanophase ferric oxide) if a second broad peak near 0.25 nm is also present. This peak is not apparent, but it may be obscured beneath the magnetite 0.252 nm peak. Because of the broad and strongly overlapping peaks, it is not possible to provide quantitative estimates of the relative proportions of unaltered glass, allophane, and nanophase ferric oxide (ferrihydrite). In addition to these phases, JSC Mars-1 and possibly PN-9 have a weak peak near 0.44 nm which can be assigned to hisingerite ($Fe_2O_3 \cdot 2SiO_2 \cdot nH_2O$) [e.g., *Eggleton and Tilley*, 1998] but not to halloysite ($Al_2O_3 \cdot SiO_2 \cdot 2H_2O$) because a peak near 1.0 nm is absent [e.g., *Wada and Mizota*, 1982; *Kawano et al.*, 1997; *Jeong*, 2000].

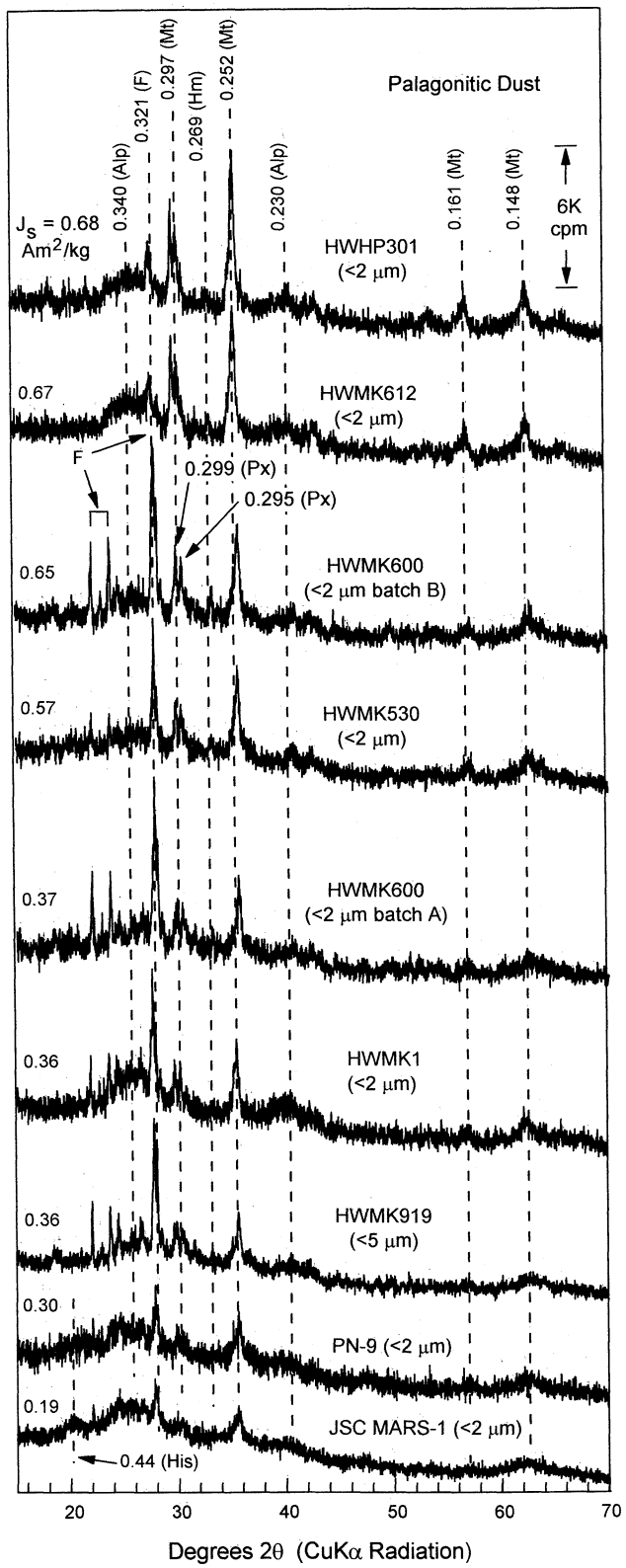

As shown in Figure 5 by differences in the intensity of the magnetite XRD peak at 0.252 nm for the magnetic and nonmagnetic separates of the <5 μm size fractions of HWMK919 and HWHP301, our magnetic separation procedure concentrated, but did not completely separate, magnetite into the magnetic fraction. This result is also observed in the magnetic data (Table 4), which show that magnetic separates have ~5 times more magnetite (i.e., ~5 times larger J_s) than nonmagnetic separates. There is no clear evidence for preferential enrichment of nonmagnetic plagioclase feldspar in nonmagnetic separates. Taken together, this behavior is consistent with the presence of composite particles that contain variable proportions of magnetic (magnetite) and nonmagnetic (e.g., silicates) phases. Only the composite particles that are most enriched in magnetite are collected in the magnetic fraction. This view is supported by direct TEM observation (see below).

In summary, the XRD evidence is that the <2 and <5 μm size fractions consist of primary minerals (plagioclase feldspar, magnetite, and minor pyroxene), minor hematite, and glass which has undergone low-temperature alteration (hydration and oxidation) to various extents. No basal reflections resulting from crystalline 1:1, 2:1, or 2:1:1 phyllosilicates were detected. Weak, broad peaks corresponding to basaltic glass, allophane, nanophase ferric oxide (possibly ferrihydrite), and hisingerite (two samples) were detected as X-ray amorphous phases.

According to *Kawano et al.* [1997], alteration of glass generally leads to the formation of phyllosilicates via several steps: (1) formation of a thin flaky or film-like noncrystalline aluminum hydroxide; (2) transformation of Al-hydroxide to irregularly aggregated Al-Si-Fe rich fibrous material; (3) morphological changes of irregularly aggregated Al-Fe-Si rich fibers to rounded aggregates; (4) development of halloysite-like curled domains in rounded aggregates with successive decrease in Fe content; and (5) growth of spherical halloysite with typical habit of circular interior texture. The nature of the phyllosilicate is determined by the mole ratio of Si/(Al+Fe) in the glass and on the existence of a phyllosilicate with the appropriate composition. If Si/(Al+Fe) ~1, then the resultant phyllosilicate is 1:1 type (e.g., halloysite), and if the ratio is ~2, then the resultant phyllosilicate is 2:1 type (e.g., smectite) [*Eggleton*, 1987]. Noncrystalline, hollow-packed spheres have been reported as precursors to phyllosilicates during the

Figure 3. XRD powder patterns (15°-70° 2θ) for the <2 or <5 μm fraction of palagonitic dust. The crystalline components (sharp peaks) consist of plagioclase feldspar (F; 0.321 nm), magnetite (Mt; 0.297, 0.252, 0.161, and 0.148 nm), and pyroxene (Px; 0.299 and 0.295 nm). The large broad humps near 0.34 and 0.23 nm are consistent with allophane (Alp). The broad peak near 0.15 nm (also contributes at 0.25 nm) is consistent with a nanophase ferric oxide (probably ferrihydrite). The broad peak near 0.44 nm for JSC Mars-1 and probably PN-9 indicates the presence of hisingerite (His; also contributes at 0.35, 0.26, 0.17, and 0.15 nm). All peak positions are in units of nanometers. CPM, counts per minute.

Table 4. Magnetic Parameters and Reflectivity at 750 nm for Palagonitic Dust at 293 K[a]

Dust Sample	Size Fraction	J_s, Am^2/kg	χ_{lf}, 10^{-6} m^3/kg	λ, Earth, T^2/m	λ, Mars, T^2/m	Reflectivity at 750 nm
		Palagonitic Dust (Unheated)				
HWHP301	<2 μm	0.68	15.5	0.79	0.30	0.370
HWHP301	<5 μm, magnetic	1.61	21.3	0.58	0.22	0.321
HWHP301	<5 μm, nonmagnetic	0.31	5.1	2.41	0.91	0.510
HWMK1	<2 μm	0.36	4.3	2.88	1.09	---
HWMK530	<5 μm	0.57	8.5	1.45	0.55	0.378
HWMK600	<2 μm, batch A	0.37	5.5	2.24	0.85	0.482
HWMK600	<2 μm, batch B	0.65	9.0	1.37	0.52	0.434
HWMK612	<2 μm	0.67	13.4	0.92	0.35	0.303
HWMK919	<5 μm	0.36	4.3	2.88	1.09	0.573
HWMK919	<5 μm, magnetic	1.25	12.3	1.00	0.38	0.405
HWMK919	<5 μm, nonmagnetic	0.27	3.2	3.85	1.45	0.584
JSC MARS-1	<2 μm	0.19	3.4	3.62	1.37	0.492
PN-9	<2 μm	0.30	4.3	2.86	1.08	0.472
		Palagonitic Dust (Heated at 495±10 °C)				
HWHP301	<2 μm	1.08	54.7	0.23	0.09	0.655
HWMK600	<2 μm, batch B	0.82	20.8	0.59	0.22	0.555

[a]Note: $\lambda \equiv g\mu_0/\chi_{lf}$, where g is the acceleration due to gravity (9.8 m/s^2 and 3.7 m/s^2 for the Earth and Mars, respectively), μ_0 is a constant equal to $4\pi \times 10^{-7}$ Vs/(Am), and χ_{lf} is the low-field magnetic susceptibility (units of m^3/kg) [*Madsen et al.*, 1999].

hydration of feldspar and some volcanic glasses [*Eggleton and Keller,* 1982; *Tazaki*, 1986; *Tazaki and Fyfe,*1987; *Eggleton*, 1987]. *Tazaki et al.* [1989] reported the formation of regions of crystallite domains in truly noncrystalline glass matrices as the first step of aqueous alteration.

The glass alteration in palagonitic dust studied here has not proceeded into the phyllosilicate stage. Samples PN-9 and JSC Mars-1 are the most evolved toward phyllosilicates because of the detection of hisingerite by the 0.44 nm XRD peak and the rare observation of spheroidal halloysite by TEM (see below). The <5 μm size fraction of a palagonitic tephra sample from Haleakala Volcano studied by *Cooper and Mustard* [1999] has also not evolved to the phyllosilicate stage (on the basis of undetected basal reflections from phyllosilicates); their tephra also does not show XRD evidence for crystalline phases like feldspar and magnetite/titanomagnetite. All our palagonitic dust samples are less evolved than (1) the soils which were collected from high rainfall areas on the island of Hawaii (100-380 cm/yr) and have gibbsite, halloysite, and low SiO_2 concentrations (~5-38 wt % on a volatile-free basis) [*Parfitt et al.*, 1988], (2) the hydrothermally altered, phyllosilicate-rich tephra from the summit region of Mauna Kea [*Ugolini*, 1974], and (3) the phyllosilicate-bearing altered vitric tephras associated with Kilauea Volcano (island of Hawaii) [*Schiffman et al.*, 2000].

3.3. Magnetic Properties

Saturation magnetization J_s and low-field magnetic susceptibility χ_{lf} are two important characterizing parameters for magnetic materials. J_s is the maximum magnetic moment that a ferromagnetic material can have in an applied magnetic field; paramagnetic materials (e.g., Fe^{2+} silicates like olivine and pyroxene) have $J_s = 0$. Values of J_s are material properties of ferromagnetic materials (e.g., J_s ~ 218 and 92 Am^2/kg for α-Fe^0 and magnetite, respectively [e.g., *Nagata,* 1961]), so the J_s for a complex geologic sample can be expressed as the concentration of a particular magnetic material in the sample if the identity of that material is known. In any case, sample J_s can be expressed as the equivalent concentration of a ferromagnetic material required to produce the sample J_s. The magnetic susceptibility is the slope of the magnetization curve as a function of applied magnetic field. For paramagnetic materials, the (paramagnetic) susceptibility is independent of applied field. The low-field magnetic susceptibility for a ferromagnetic material is measured in applied magnetic fields that are very much less than those required to achieve the maximum magnetic moment, is generally much larger than the paramagnetic susceptibility of a pure paramagnetic material, and varies with the particle diameter and shape and magnetic interactions between grains. Detailed discussions of magnetic parameters are given in the literature [e.g., *Nagata*, 1961; *Stacey and Banerjee*, 1974; *Moskowitz and Hargraves*, 1982].

Values of J_s and χ_{lf} at 293 K for palagonitic dust are compiled in Table 4. Figure 6 is a correlation of these two parameters for palagonitic dust and for other samples of palagonitic tephra [*Morris et al.*, 2000]. Note that all samples follow the same correlation and that $J_s \cong 0.10\chi_{lf}$ when J_s and χ_{lf} are in units of Am^2/kg and 10^{-6} m^3/kg, respectively. The magnetic and nonmagnetic separates of the <5 μm size fractions of HWHP301 and HWMK919 have the highest and among the lowest values, respectively, of the magnetic parameters for the dust samples. Using 92 Am^2/kg for the J_s of chemically pure and stoichiometric magnetite, the dust samples (unheated and not magnetically separated) have the equivalent of ~0.2 to 0.7 wt % magnetite. The actual amount of Fe-Ti spinel is probably somewhat higher because the J_s of Fe-Ti spinels is lower than that of pure magnetite [e.g., *Nagata,* 1961].

Heating palagonitic dust samples HWHP301 and HWMK600 (batch B) to ~495°C enhanced their magnetic properties. J_s and χ_{lf} increased by factors of ~1.4 and ~3,

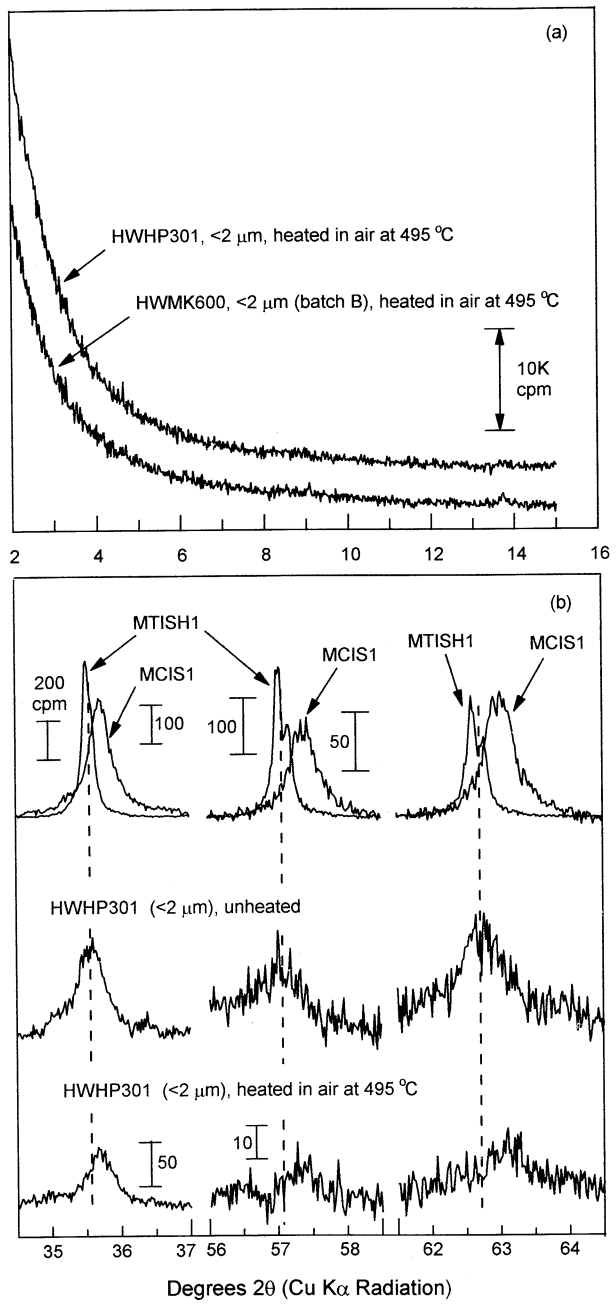

Figure 4. XRD powder patterns (unoriented mounts) of HWHP301 (<2 μm) and HWMK600 (<2 μm batch B) in selected regions showing that heating at ~495°C (a) did not crystallize phyllosilicates and (b) oxidized the magnetite to maghemite. For reference, data for magnetite (MTISH1) and maghemite (MCIS1) powders [described by *Morris et al.*, 2000] are shown in Figure 4b. CPM, counts per minute.

respectively (Table 4). We would expect the product of heating to still be magnetic, because the XRD results showed that the magnetite oxidized to maghemite, which is also a strongly magnetic mineral. However, the J_s for maghemite (~50-74 Am^2/kg) is normally less than that for chemically pure and stoichiometric magnetite, suggesting that product of heating should be less magnetic. We suggest three possible explanations, the first being increased magnetization associated with unmixing of the titanomaghemite that formed during oxidation [e.g., *Johnson and Merrill,* 1973]. Or, there may be sufficient carbon (organics) in our samples for the np-Ox to reduce to magnetite and subsequently oxidize to maghemite. Reduction of ferrihydrite to magnetite in the presence of carbon has been demonstrated in the laboratory [*Campbell et al.*, 1997]. Lastly, dehydration and/or dehydroxylation of np-Ox during heating may have produced a different form (possibly nanophase hematite [*Morris et al.*, 1989]) that is more magnetic than its precursor. At present, we cannot distinguish which alternative or combination thereof is applicable.

3.4. Mössbauer Spectroscopy

Mössbauer spectra (273 K) for the <2 μm size fraction of six palagonitic dust samples are shown in Figure 7. The samples are ordered as in Figure 3 (decreasing values of J_s), and the spectra are scaled so that the prominent doublet has the same intensity in each spectrum. The doublets (IS~0.34 mm/s and QS~0.80 mm/s, where IS is isomer shift and QS is quadrupole splitting) result from octahedrally coordinated ferric iron and, because we do not know the hydration state of the ferric iron, are associated with compositions between nanophase hematite and 2-XRD-line ferrihydrite (collectively, np-Ox) [e.g., *Morris et al.*, 1993, 2000]. These phases are not

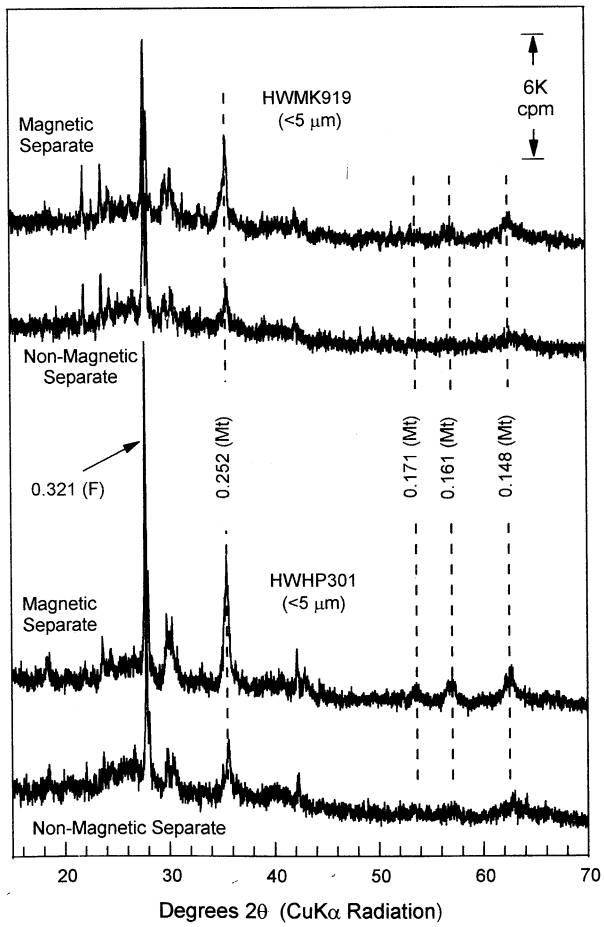

Figure 5. XRD powder patterns (15°-70° 2θ) for magnetic and nonmagnetic separates of the <5 μm size fraction of HWMK919 and HWHP301. Peaks corresponding to magnetite are present in both separates but are more intense in magnetic separates. All peak positions are in units of nanometers. CPM, counts per minute.

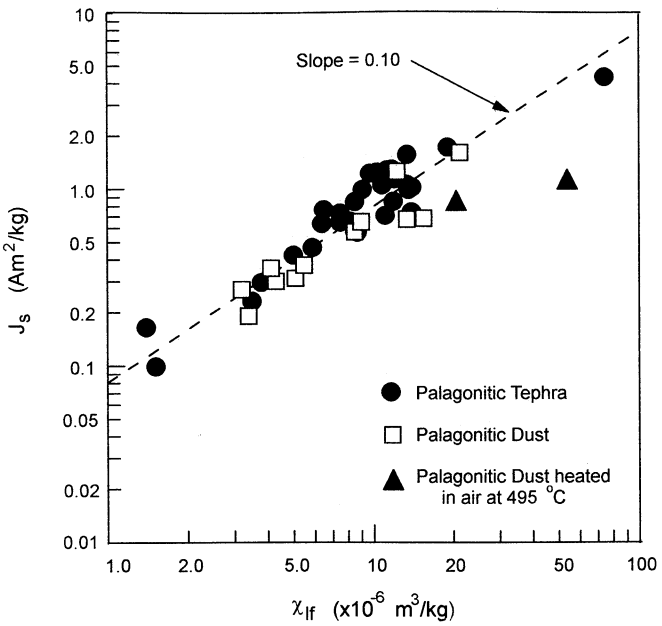

Figure 6. Saturation magnetization J_s versus low-field magnetic susceptibility χ_{lf} at 293 K for palagonitic tephra [from *Morris et al.*, 2000], palagonitic dust, and heated (~495°C) palagonitic dust. Palagonitic tephra and palagonitic dust have comparable ranges for the two magnetic parameters.

distinguishable by XRD because both have two broad XRD lines centered near 0.25 and 0.15 nm [*Morris et al.*, 1991]. Hisingerite, for which there is XRD evidence in samples PN-9 and JSC Mars-1 and which may exhibit a XRD pattern similar to 2-XRD-line ferrihydrite [*Farmer*, 1992], would also contribute to the ferric doublet.

Magnetic splitting (sextet) is also clearly present for all samples except PN-9 and JSC Mars-1; the peak positions and intensities correspond to magnetite and hematite in different proportions. HWHP301 and HWMK612 are enriched in magnetite relative to hematite and vice versa for HWMK600 and HWMK530. Qualitatively, sextet intensity decreases (relative to constant doublet intensity) from HWHP301 through JSC Mars-1, the same order as the decrease in J_s.

Other iron-bearing components are indicated by the peaks centered between ~2.0 and 2.7 mm/s (most evident in HWMK1, HWHP301, and HWMK612). We attribute them to the high-velocity peaks of doublets from octahedrally coordinated ferrous iron in olivine, pyroxene, and/or glass, as reported previously for Mauna Kea palagonitic tephra [*Morris et al.*, 1993, 2000; *Bell et al.*, 1993].

In summary, Mössbauer spectroscopy shows for palagonitic dust that np-Ox is the major iron-bearing phase and that variable proportions of hematite and magnetite are present as magnetically ordered phases. HWHP301 and HWMK612 have the highest proportion of magnetically ordered oxides, and JSC Mars-1 and PN-9 have the lowest.

3.5. Visible and Near-IR Reflectance Spectroscopy

Visible and near-IR reflectivity spectra for mixtures of palagonite (HWMK600) and smectite (SWa-1) show that the smectite is not spectrally detected on the basis of the 1400 and 1900 nm bands for concentrations less than ~10 wt % (Figure 8), a detection limit about a factor of 3-10 times larger

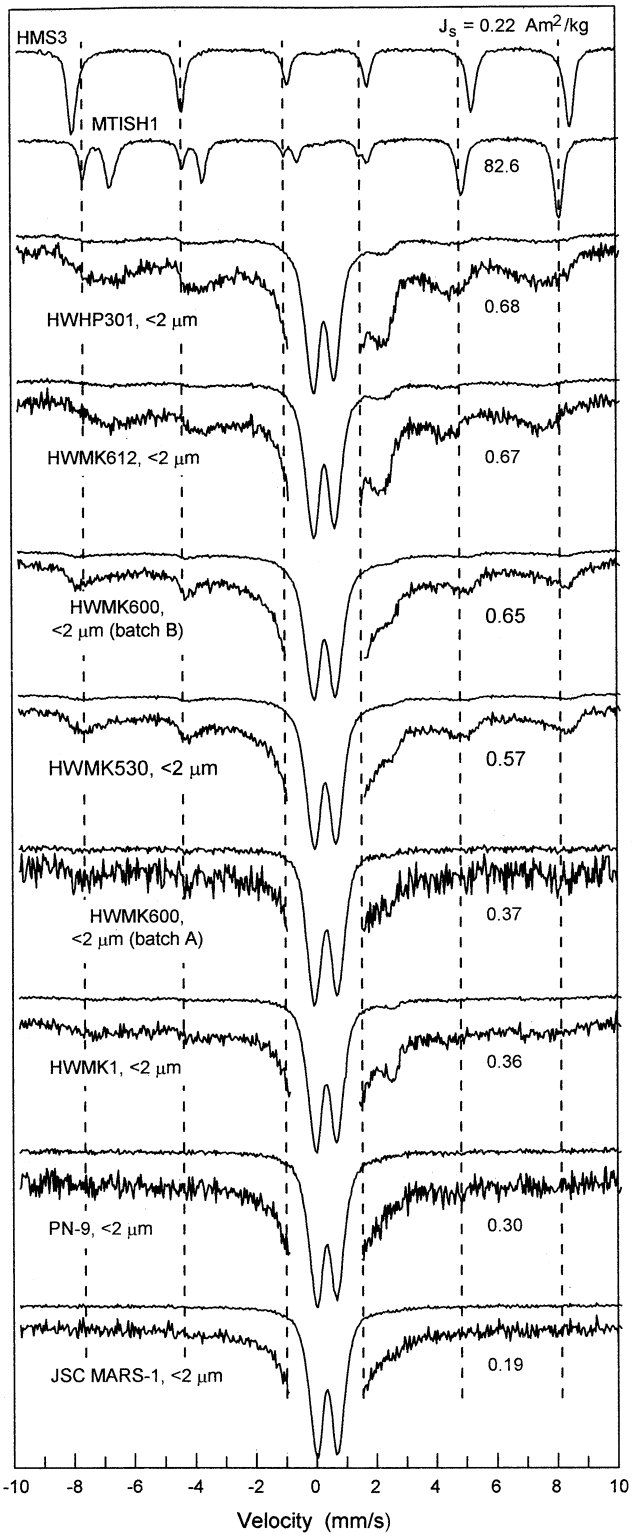

Figure 7. Transmission Mössbauer spectra (293 K) of palagonitic dust are dominated by a central doublet (IS~0.33 mm/s and QS~0.8 mm/s) resulting from octahedrally coordinated ferric iron associated with nanophase ferric oxide. Magnetic splitting resulting from magnetite and hematite are also present with decreasing intensity from HWHP301 through PN-9 and JSC Mars-1 where the sextets are not detected. Note that the saturation magnetization J_s decreases in the same order, corresponding to the decrease in the abundance of strongly magnetic magnetite. Mössbauer spectra for pure hematite (HMS3 [*Morris et al.*, 1985]) and magnetite (MTISH1 [*Morris et al.*, 2000]) are shown for reference. The *y* axis is in units of counts.

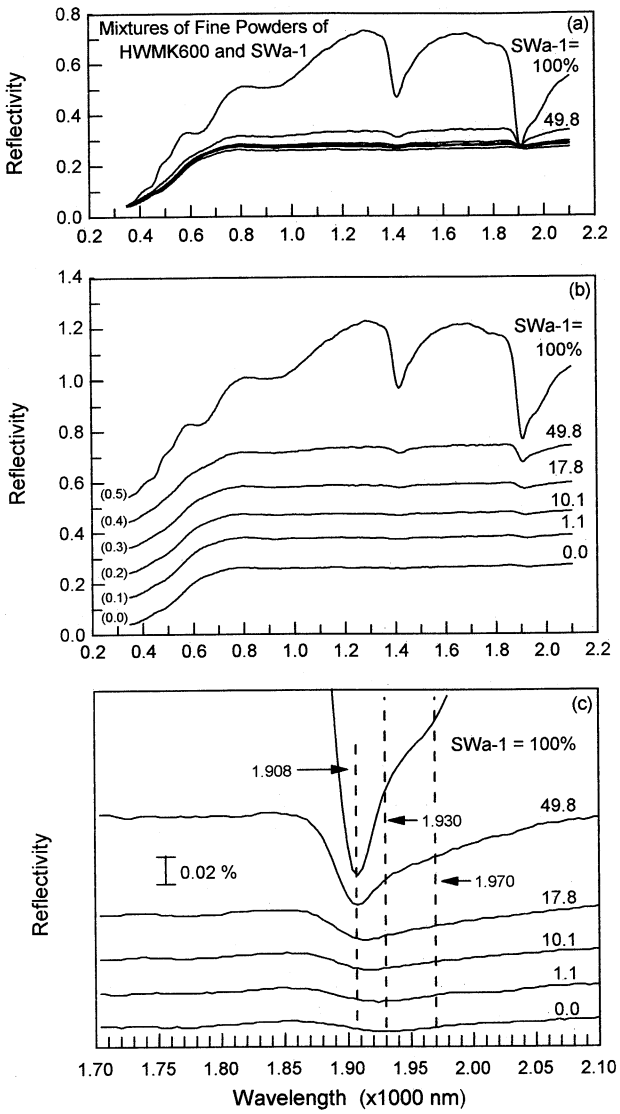

Figure 8. Visible and near-IR reflectivity spectra (293 K) for mixtures of HWMK600 (<1 mm powder) and smectite SWa-1. (a) Unstacked and (b) stacked spectra showing that the smectite does not significantly change reflectivity for samples with ≲10 wt % smectite. The spectral features near 1400 and 1900 nm result from combination/overtones of H_2O and OH fundamental vibrations. (c) Enlarged view of the 1900 nm region. Note the increase in width and shift of minimum to longer wavelengths with increasing palagonite content. Smectite dominates the 1900 nm spectral feature for >50 wt % smectite.

than the XRD detection limit for the same mixtures (Figure 1). The band near 1900 nm, which occurs with different intensity and slightly different positions in each end-member (1910 nm for SWa-1 and 1930 nm for HWMK600), is the more sensitive indicator for the presence of smectite. The band positions agree with those reported by *Bishop and Pieters* [1995] for montmorillonite and a palagonitic soil from Haleakala Volcano (island of Maui, Hawaii).

The bands near 1400 and 1900 nm result from overtones and combinations of fundamental vibrations that occur at longer wavelength. For water vapor, symmetric OH stretching (ν_1), asymmetric OH stretching (ν_3), and H-O-H bending (ν_2) fundamental vibrations occur at 2.738, 2.663, and 6.269 μm, respectively. The overtone and combination bands near 1400 and 1900 nm include $\nu_1+\nu_3$ (1350 nm), $2\nu_2+\nu_3$ (1440 nm), and $\nu_2 + \nu_3$ (1869 nm) [e.g., *Hunt and Salisbury*, 1970; *Clark et al.*, 1990]. In minerals, one or more bands are often present near these wavelengths, corresponding to OH and H_2O in multiple environments. For smectite, *Bishop et al.* [1994] assigned positions at 1910 and 1970 nm to combinations of the H-O-H bending and OH stretching fundamentals associated with bound (interlayer) and adsorbed H_2O, respectively. Presumably, the same combination band in palagonite occurs in a different place (1930 nm) because the environment for H_2O is different. This is reasonable because palagonite, being hydrated basaltic glass, has no structural exchange sites where cations reside as does smectite. Even in smectites, the position of the H-O-H fundamental varies in response to the polarization state of water, which depends on the nature of the cation at the exchange site and the number or water molecules surrounding it, which is a function of the partial pressure of water [e.g., *Johnston et al.*, 1992; *Bishop and Pieters*, 1995].

Representative visible and near-IR reflectivity spectra (350-2100 nm) for palagonitic dust are shown in Figure 9. All have the ferric absorption edge between ~350 and 750 nm and the relatively flat reflectivity at longer wavelengths that are characteristic of Hawaiian palagonitic tephra [e.g., *Singer*, 1982; *Morris et al.*, 1990, 1993, 2000; *Bell et al.*, 1993]. *Morris et al.* [2000] observed an inverse correlation between the reflectivity at 750 nm, which is representative of the general magnitude of reflectivity in the region 750-2100 nm, and the low-field magnetic susceptibility for dust size fractions (<2, 2-5, and <5 μm) of palagonitic tephra. Because magnetite is black and magnetic, the inverse correlation was attributed to increasing concentrations of the black magnetic pigment in otherwise bright nonmagnetic or weakly magnetic material. Figure 10 shows that the correlation R750 and χ_{lf} reported by *Morris et al.* [2000] is preserved when the data for unheated dust samples from this study (Table 4) are included. Note that the values of both R750 and χ_{lf} for the bulk <5 μm size fractions of HWHP301 and HWMK919 are intermediate to the corresponding values for their magnetic and nonmagnetic separates (Table 4).

In Figure 10 the two data points for the heated (495°C) samples of palagonitic dust HWHP301 and HWMK600 (batch B) are off the trend of the unheated samples in the direction of brighter and more magnetic (Figure 9). Possible explanations for the increase in magnetic properties were discussed above. An obvious explanation for the increase in reflectivity is oxidation of black magnetite to brighter maghemite. However, both heated tephra samples are more reflective at 750 nm than the pure maghemite powders, suggesting that other factors contribute to brightening of the heated powders.

3.6 Transmission Electron Microscopy

The data discussed above show that phyllosilicate-poor palagonitic dust from Mauna Kea is a mineralogically complex assemblage that includes magnetite, plagioclase, pyroxene, glass, and alteration products of the glass. These data do not show by direct observation whether these phases are present as discrete particles or as components of composite particles. We used TEM to provide information about the physical arrangement of the phases, which we

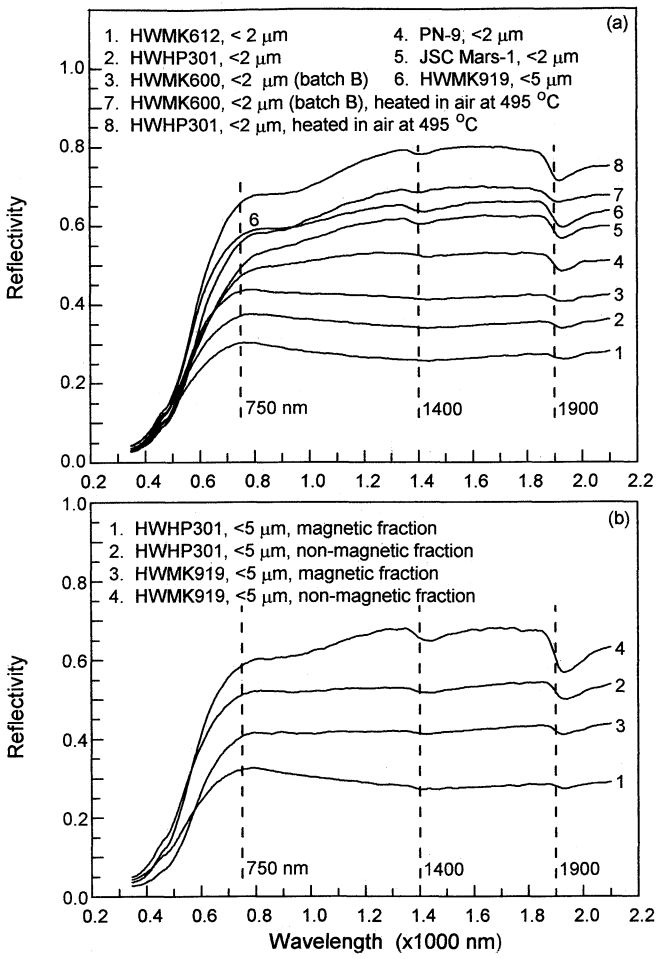

Figure 9. Visible and near-IR reflectivity spectra (293 K) for palagonitic dust. All spectra are characterized by a ferric absorption edge extending from ~400 to 800 nm. These spectra show that (a) heating palagonitic dust increases the reflectivity in the near-IR and (b) nonmagnetic fractions are more reflective in the near-IR than the magnetic fraction from the same sample because of higher magnetite concentrations in the magnetic separates.

identified by selected area electron diffraction and elemental analysis.

Low-magnification views of HWMK600 (Figure 11a) and HWHP301 (Figure 11b) are typical and show that dust particles consist largely of a Al-Fe-Si-rich noncrystalline matrix (in the dark field TEM image) either in compact fragments (Figure 11a) or porous clusters (Figure 11b) within which are "phenocrysts" of silicate mineral fragments (plagioclase and pyroxene) and heterogeneously distributed patches that contain high number densities of crystalline Fe-Ti oxide particles. Mineral grains relatively free of matrix material are also present. High-magnification views show that the size distribution of oxide particles within patches is relatively narrow, but the average oxide particle diameter varies from patch to patch. Patches with embedded Ti-bearing magnetite in several diameter ranges are shown in Figures 12a-12d. Occurrences with 5-20 nm oxide particles are the most common and were found in all samples. Larger (>50 nm) and relatively isolated oxide particles were also present (Figure 12a). Selected area electron diffraction patterns of the regions that contain the 5-20 nm oxide particles from HWMK600 (Figure 12b) and the 50-150 nm oxide particles from HWMK1 (Figure 12d) are shown in Figures 12e and 12f. The electron diffraction pattern for HWMK600 consists of incomplete rings made of spots at 0.29, 0.25, 0.21, 0.17, and 0.15 nm. The spottiness of the rings results from a large but finite number of randomly oriented Ti-bearing magnetite crystals within the electron beam. The electron diffraction pattern for spinel particles in HWMK1 shows a ring pattern with well-developed spots corresponding to a relatively small number of larger well crystalline, randomly oriented magnetite crystals within the electron beam. Although we were not able to accurately determine the elemental composition of the 5-150 nm spinel particles because of their small size, they invariably contained Ti, and the Ti content seemed to decrease with decreasing diameter (data not shown). The 50-150 nm spinel particles in Figure 12d have x=0.28±0.05 ($Ti_xFe_{(3-x)}O_4$) (data not shown). The magnetite particles in palagonite are similar in appearance to magnetite particles observed in some carbonaceous chondrites but are compositionally different because they contain Ti and the chondritic magnetite particles do not [e.g., *Kerridge*, 1970; *Kerridge et al.*, 1979].

Representative examples of noncrystalline matrix in regions relatively free of crystalline minerals are shown in Figure 13. Fibrous-appearing regions (not glass) were amorphous to the electron beam (tested by dark field imaging and electron diffraction), were rich in Al, Si, and Fe and with minor Ti, and were abundant in all samples (Figures 13a, 13b, and 13c). The fine fibrous nature of the TEM image suggests short-range reorganization of the glass structure, possibly resulting from glass hydration, oxidation of ferrous to ferric iron, and precipitation of np-Ox particles. The lighter areas

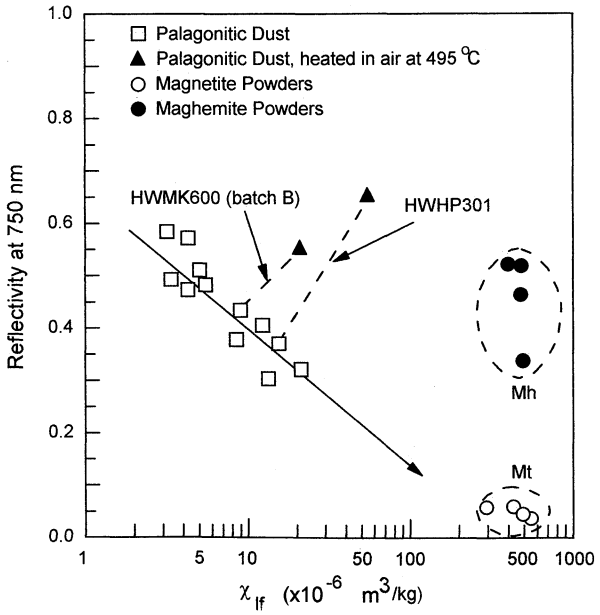

Figure 10. Reflectivity at 750 nm as a function of low-field magnetic susceptibility. The reflectivity at 750 nm decreases with increasing concentration of magnetite (increasing magnetic susceptibility) and, qualitatively, extrapolates to fine powders of magnetite (arrow). Data for maghemite (Mh) and magnetite (Mt) powders are from *Morris et al.* [2000].

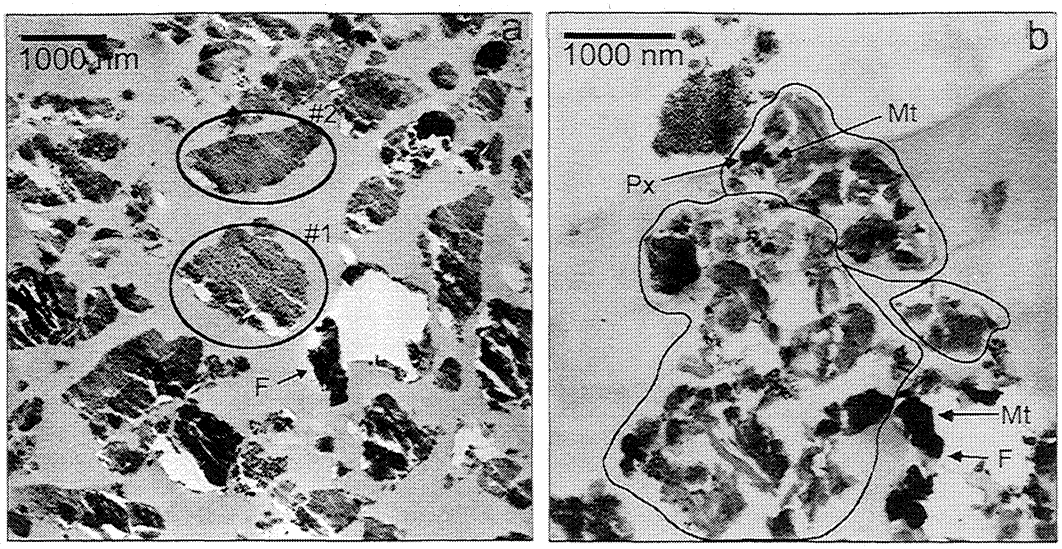

Figure 11. Transmission electron micrographs of thin-sectioned palagonitic dust (<2 μm). (a) Composite particles from HWMK600 are particles of plagioclase (F) and Ti-bearing magnetite (Mt) occurring as "phenocrysts" within a Al-Si-Fe noncrystalline matrix. Note that some composite particles appear to be "peppered" with the spinel particles (particle 1). Much smaller scale peppering (1-5 nm) in other particles (particle 2) probably corresponds to np-Ox particles. Individual mineral grains with little adhering matrix are also present. (b) Loosely held clusters from HWHP301 that contain larger spinel particles than those in Figure 11a, plagioclase feldspar, pyroxene (Px), and fibrous amorphous Al-Si-Fe silicates, and amorphous areas containing np-Ox. Solid lines enclose porous particles.

(less electron dense) probably correspond to the allophane identified in the XRD patterns, and the darker areas (more electron dense) probably correspond to areas enriched in np-Ox particles. We interpret relatively uniform areas (e.g., Figure 13b) as hydrated glass that has not undergone appreciable short-range reorganization. Spheroidal structures (Figure 13d) are rare and found only in PN-9 and JSC Mars-1. We identify these structures as spheroidal halloysite because they have Al and Si; the fibrous material between them is rich in Fe and may correspond to hisingerite. We also observed (not shown) only in these two samples incipient organization of lamellae to form spherical structures similar to that reported by *Tazaki et al.* [1989]. Unaltered or weakly altered glass was identified in many areas by the "chatter" pattern perpendicular to the cut direction that results when the diamond knife cuts brittle glass during preparation of samples for TEM analysis (Figures 13c and 13d).

3.7. Summary of Palagonitic Dust Mineralogy

Taken together, XRD, Mössbauer, magnetic, and reflectivity data show that our palagonitic dust is a complex assemblage consisting of plagioclase feldspar, magnetite, pyroxene, and olivine as crystalline phases and glass, np-Ox, and incipient phyllosilicates (allophane, fibrous structures, and rare hisingerite/halloysite) as X-ray amorphous phases. All X-ray amorphous phases except glass are aqueous alteration products. No well crystalline phyllosilicates were detected. All crystalline phases plus glass were formed during cooling of silicate liquids (lithogenic in origin). The small size of the spinel particles and their heterogeneous distribution in patches with different average spinel particle diameters imply crystallization at variable cooling rates during or shortly after volcanic eruption and deposition. As summarized by *Morris et al.* [1993], the composition of micron-sized and larger titanomagnetite grains within large (>20 μm) tephra particles is $Ti_xFe_{(3-x)}O_4$ ($0.35<x<0.60$). The 50-150 nm spinel particles in palagonitic dust have less Ti ($x=0.28\pm0.05$), and, qualitatively, the Ti content seems to decrease with decreasing spinel-particle diameter. On the basis of values of J_s, bulk palagonitic dust samples have 0.2-0.7 equivalent weight percentage magnetite.

TEM studies show by direct observation that individual palagonitic dust particles are mostly composite particles of more than one phase. The general observation is that crystalline phases are embedded within or have adhering basaltic glass and/or its X-ray amorphous alteration products. In particular, the magnetic 5-150 nm titanomagnetite particles are heterogeneously distributed within other materials. The implication (and observation) is that it is not possible to obtain pure titanomagnetite mineral separate from palagonitic dust using only magnetic separation procedures. The magnetic properties of dust particles are not uniform, presumably in response to variable contents of Ti-bearing magnetite, because we were able to use magnetic separation procedures to obtain separates that were more and less magnetic than the bulk dust.

4. Pathfinder Magnet Array Experiments on Mauna Kea Volcano

4.1. Photographic Observations

Plate 1 shows photographic documentation of nine Magnetic Array experiments done on Mauna Kea Volcano. Wind direction and velocity and time relative to the start of each experiment are indicated. Arrows pointing up and down denote wind directions from the front and back of the array,

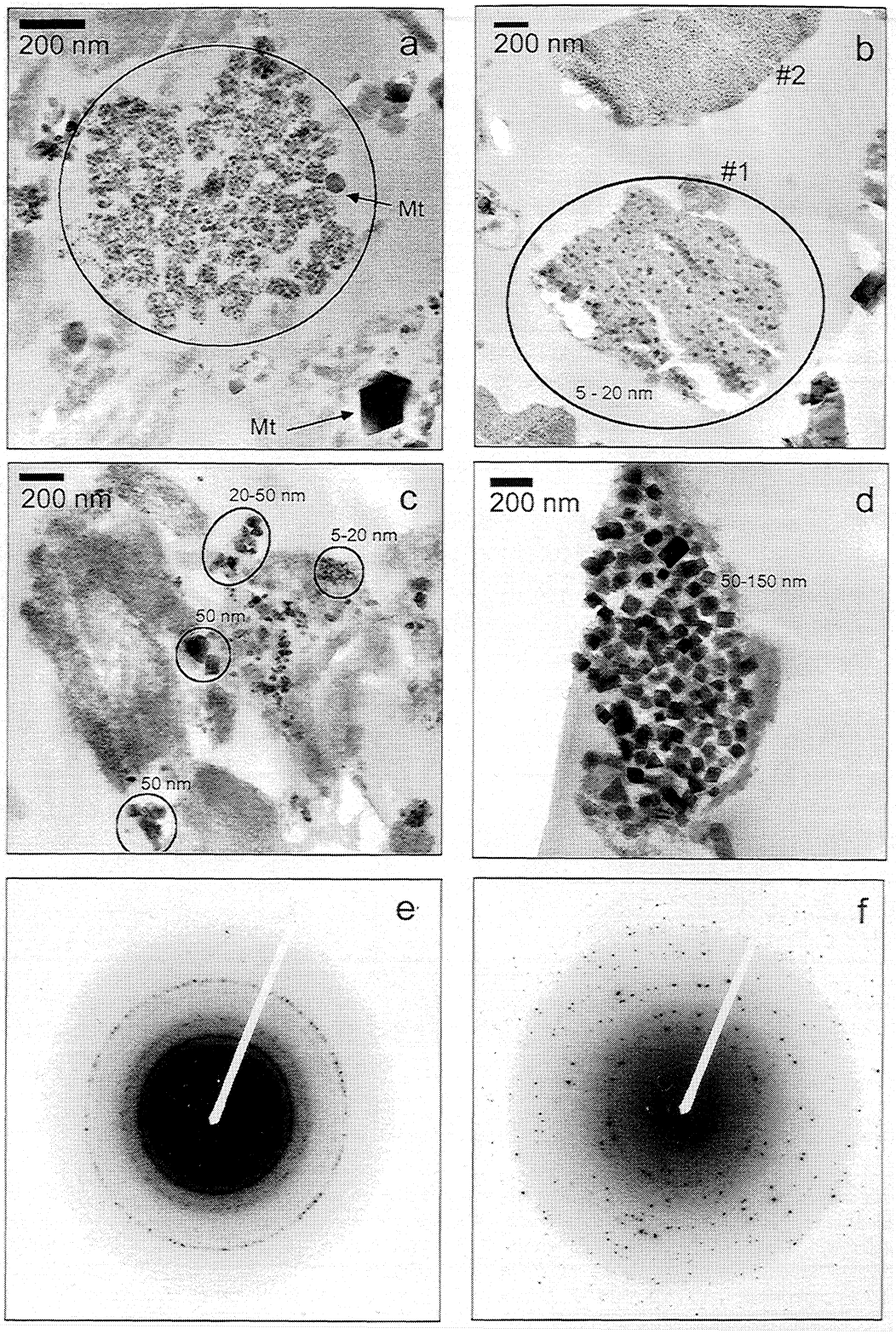

Figure 12. Transmission electron micrographs of thin-sectioned palagonitic dust (<2 μm). (a) Porous particle from HWHP301 with uniform 5-20 nm spinel grains distributed throughout the matrix. Note the few larger spinel grains in the section. (b) Enlarged view of HWMK600 particle 1 in Figure 11a showing the peppering of 5-20 nm spinel particles in the composite particle. (c) A region of HWMK612 peppered with spinel particles having different size distributions. (d) Dust particle from HWMK1 with euhedral magnetite crystals in the diameter range 50-150 nm. (e) Electron diffraction pattern particle 1 from HWMK600 in Figures 11a and 12b. Incomplete rings made of spots are present at 0.29, 0.25, 0.21, 0.17, and 0.15 nm, corresponding to many, small, and randomly oriented magnetite particles within the diameter of the electron beam. Spots correspond to a discrete number of larger spinel particles. Np-Ox (e.g., ferrihydrite) would also contribute the diffuse ring near 0.25 and 0.15 nm. (f) Electron diffraction pattern of the euhedral spinel particles from HWMK1 in Figure 12d. The rings of discrete spots result from a finite number of discrete spinel crystals within the electron beam. X-ray dispersive analysis shows that the spinels are titanomagnetite with x=0.28±0.05 (data not shown).

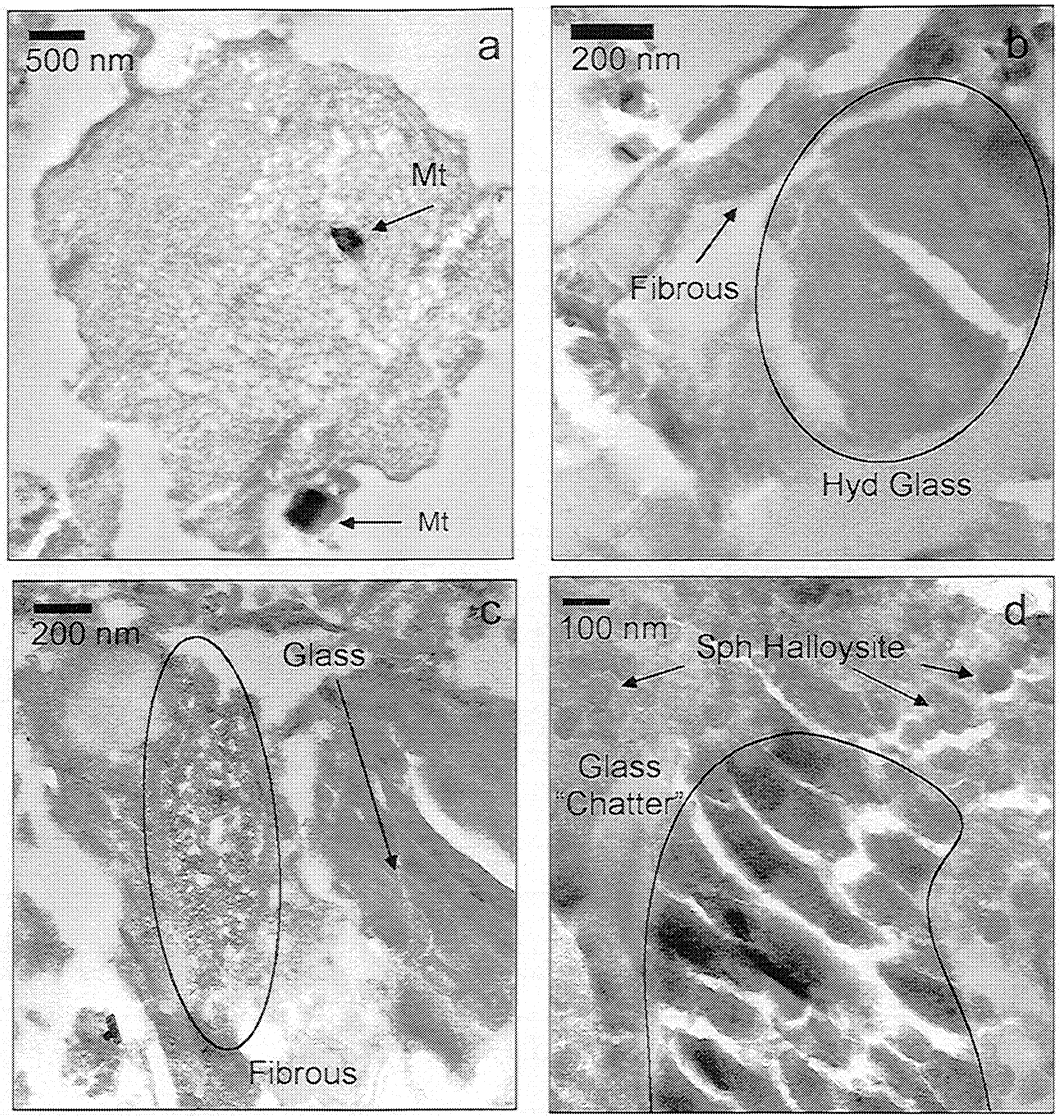

Figure 13. Transmission electron micrographs of thin-sectioned palagonitic dust (<2 μm) for regions relatively free of crystalline materials. (a) Fibrous-appearing region from HWMK1 with two embedded magnetite crystals. The density of fibers increases from left to right, corresponding to increasing alteration of the glass. (b) Fibrous region from HWHP301. (c) Fibrous and glass region from JSC Mars-1. (d) Region from PN-9 showing glass and halloysite. Glass is recognized by the "chatter" pattern created when the diamond knife cuts brittle glass during sample preparation.

respectively. A range of velocities is given because the wind velocity was always variable during an experiment. We estimate that the wind direction was constant to within ±20° from the indicated direction. A wind velocity meter was not available for experiment HWMK8MA00. Chemical compositions of the reference palagonitic tephra (<1 mm) for MA experiments are given in Table 3.

Experiments HWMK8MA00 and HWMK9MA19 (Plates 1a and 1b) were done near the entrance to the Very Long Baseline Array (VLBA) telescope compound on the north side of the road. The patterns developed on the two MAs are different, but in each case dust was collected by all five magnets. Reasonably uniform "target" patterns are particularly well developed in experiment HWMK8MA00. Irregular patches of dust appear on magnets 4 and 5 of experiment HWMK9MA19. We observed this kind of behavior when a gust of wind (presumably with velocity gradients) selectively lifted dust from the array. The patches then become places where it is easier for incoming dust particles to stick, as shown by the increase in size of the patches in the 16 min picture relative to the 8 min picture.

Experiment HWMK9MA16 was done west of the Visitor's Center on the south flank of Puu Kilohana cinder cone (Plate 1c). The target pattern is clearly present on all five magnets. Experiments HWMK9MA23 and HWMK9MA25 (Plates 1d and 1f) were done on the south side of the road to the VLBA telescope, part way up the north flank of an unnamed cinder cone. During these experiments the maximum wind velocity was about twice that for the other experiments (~8 m/s compared to ~4 m/s). For experiment HWMK9MA23 the wind was from the front, dust was collected by only the four strongest magnets, and the efficiency of collection by the

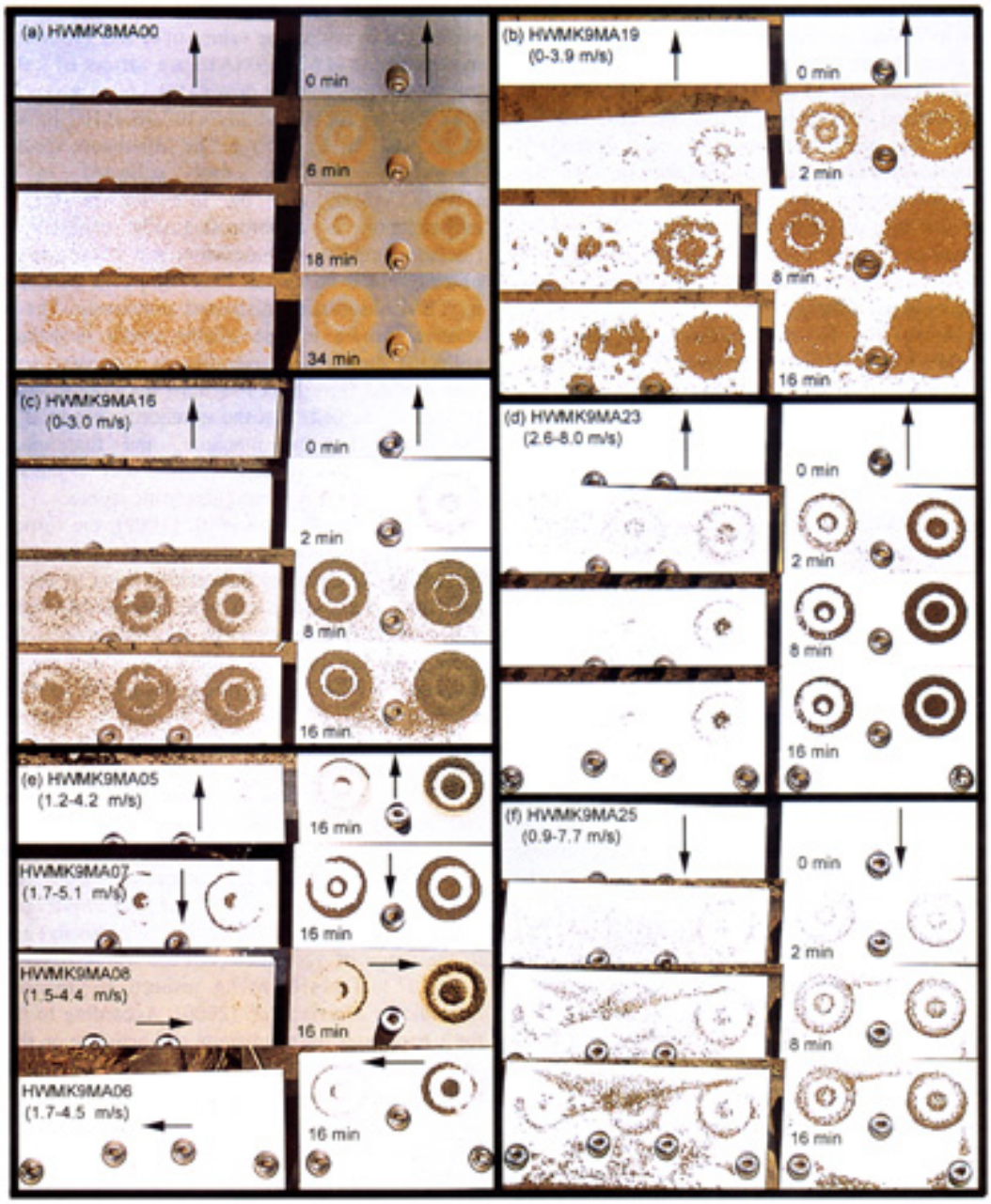

Plate 1. Magnetic Array experiments on Mauna Kea Volcano. Arrows indicate wind direction. Experiments (a) HWMK8MA00, (b) HWMK9MA19, and (c) HWMK9MA16 show dust collection by all five MA magnets; the wind speed was not measured for Plate 1a but was about 0-4 m/s for Plates 1b and 1c. Experiment (d) HWMK9MA23 was conducted with about twice the wind speed in Plates 1b and 1c. Dust was collected by five magnets at 2 min (just visible on magnet 5). At 8 and 16 min, dust is not visible on magnet 5 but has continued to collect on the other magnets, presumably in response to increasing wind speed during the experiment. Experiment (e) HWMK9MA05-08 show that, except for wind from the back, dust is preferentially collected by the downwind side of the magnets if the wind is sufficiently strong. In experiment (f) HWMK9MA25 the wind speed was comparable to Plate 1d, but wind direction was incident from the back of the MA. In this orientation the back of the MA shields the magnet collection surface from the wind, lowering the wind speed at the collection surfaces. Dust was collected by five magnets, and the "v" pattern at the top of each subarray is typical for wind blowing in this orientation. Experiments in Plates 1a and 1b were done at the same place on the north side of the VLBA road in 1998 and 1999, respectively. Experiments in Plates 1c and 1e were done west of the Visitor's Center on the south flank of Puu Kilohana. Experiments in Plates 1d and 1f were done on the south side of the VLBA road.

other four magnets was reduced (compare with experiment HWMK9MA16). In addition, the stronger wind did not allow as much dust to collect on the MA face at locations away from the magnets. In experiment HWMK9MA25 the wind direction was from the back of the MA, so the dust collection surface was protected from direct assault of the wind and dust. Intuitively, this orientation would produce eddies and reduced wind velocities on the front side of the MA. Dust was collected by all five magnets, and a "v-shaped" pattern of dust developed at the top of each subarray. Presumably, this pattern was produced by the wind blowing around the edges of the two subarrays, forming regions of low wind velocity mapped by the v-shaped pattern.

Plate 1e shows the 16 min pictures for four MA experiments (HWMK9MA05-08) performed at the same location as HWMK9MA16 but on a different day when the wind was stronger with no calm periods. The orientation of the wind was changed for each experiment (front, back, and each side). For all wind orientations except the back, dust was collected by the three strongest magnets. Dust was collected by four magnets for the back orientation, presumably because the wind velocity on the front of the MA was reduced, as discussed above. Thus dust was collected by fewer magnets than in previous experiments, which were five magnets for both HWMK9MA16 (Plate 1c; front wind orientation) and HWMK9MA25 (Plate 1f; back wind orientation). Also note that the v-shaped patterns did not develop on each subarray for experiment HWMK9MA07 (wind direction from the back). The results are internally consistent in that the appearance of the v-shaped pattern is consistent with low wind velocities, which would favor dust collection by all five magnets. However, they seem at odds with the higher velocity recorded for the wind in experiment HWMK9MA25. Perhaps the wind flow was more laminar (less turbulent) in the MHMK9MA25 experiment, which permitted formation of low-velocity regions on the MA surface and deposition of the v-shaped dust pattern and collection of dust by all five magnets. In other experiments with the wind direction from the back (not shown), formation of v-shaped patterns was the usual result.

Plate 1e also shows that the wind direction can influence the distribution of dust collected on the magnets. For the front and side orientations, dust is preferentially collected on the downwind side of the individual magnets. For example, the downwind sides of magnets 1 and 2 for experiment HWMK9MA05 are clearly thicker and better defined than the upwind sides. This result is probably some combination of particles being blown from one side of each magnet to the other and the slowing down (magnetic drag) of dust particles so that they can be collected on the downwind side with increased probability.

4.2. Sample Analyses

Collected mass and magnetic measurements on samples obtained from individual magnets during MA experiments are summarized in Table 5. In Figure 14 we plot the saturation magnetization as a function of low-field magnetic susceptibility for the dust collected from the MA magnets, the MA base plate, and the unheated samples of palagonitic dust discussed previously. It is evident that the MA magnets preferentially collected the more strongly magnetic particles from the incident dust. For all experiments except one (HWMK9MA19), the values of the two magnetic parameters are larger than those for bulk dust collected from MA base plates. For example, the values of J_s and χ_{lf} for collected dust in experiment HWMK9MA16 are factors of 2-3 larger than the values for incident dust (2.08-3.60 Am^2/kg compared to 1.07 Am^2/kg for J_s and $23.7x10^{-6}$-$36.4x10^{-6}$ m^3/kg compared to $12.3x10^{-6}$ m^3/kg for χ_{lf}). The Mössbauer spectra in Figure 15 show that the dust collected in experiment HWMK8MA00, and by inference in the other MA experiments, is a mineralogically complex assemblage (including np-Ox, Ti-magnetite, and olivine as iron-bearing phases) that is consistent with composite particles as shown by TEM observation discussed previously. The presence of relatively more intense olivine peaks in palagonitic dust collected during MA experiments compared to palagonitic dust derived from bulk (<1 mm) palagonitic tephra samples (Figure 7) suggests that the weathering products that include the oxides (np-Ox, hematite, and titanomagnetite) are preferentially concentrated in the <2 and <5 μm size fractions after sonication of <1 mm palagonitic tephra.

According to *Madsen et al.* [1999], the response of dust composed of composite particles having a range of magnetic properties (as does our palagonitic dust) to the MA will be such that the dust collected from successively weaker magnets will have higher values of J_s. The rationale is that only the most magnetic particles will be collected by the weakest magnet, while the stronger magnets are not so discriminating. *Madsen et al.* [1999] also calculate a relative collection efficiency for the individual magnets that is based on a λ parameter defined as $g\mu_0/\kappa_i$, where g is the acceleration due to gravity (9.8 m/s^2 for the Earth and 3.7 m/s^2 for Mars), μ_0 is a constant equal to $4\pi x10^{-7}$ Vs/(Am), and κ_i is the magnetic susceptibility. The parameter κ_i is equivalent to our parameter χ_{lf}, as can be verified by comparing values for the same minerals. Their values of κ_i for maghemite and hematite ($520x10^{-6}$ m^3/kg and $3x10^{-6}$ m^3/kg, respectively) are proximate to the range of χ_{lf} values ($401x10^{-6}$ to $496x10^{-6}$ m^3/kg and $0.15x10^{-6}$ to $1.84x10^{-6}$ m^3/kg, respectively) reported for those minerals by *Morris et al.* [2000]. According to the values of the λ parameter for maghemite and hematite on the Earth (4.2 and 0.026, respectively), maghemite would be collected by all five magnets and hematite would be collected by only the strongest one [*Madsen et al.*, 1999; Figure 7]. With one exception the values of λ for the dust collected on the MA magnets during the Mauna Kea experiments range from ~0.3 to 2.0 (Table 5), which would imply palagonitic dust collection by at most the three strongest magnets. As discussed above, dust was collected by all five magnets in many of our experiments (Plate 1).

In Figures 16a and 16b, we consider the variation of J_s, χ_{lf}, and normalized collected mass (mass collected relative to magnet 1) as a function of magnet strength. Also shown for comparison are results for a heated sample of ocher from *Madsen et al.* [1999]. Although the dust collected by the magnets in the Mauna Kea experiments is more magnetic than the corresponding bulk dust, no regular increase in either magnetic parameter with increasing magnet number (decreasing magnet strength) is observed, i.e., no magnetic sorting of the dust particles according to magnet strength. Because magnetic sorting requires a significant distribution in the values of J_s for individual dust particles (e.g., 2-12 Am^2/kg) [*Madsen et al.*, 1999], its absence implies that sufficient variability is not present. The magnetic results

Table 5. Average and Normalized Recovered Mass and Magnetic Parameters at 293 K for Dust Collected From Magnet Array Base and Individual Magnets[a]

Samples	Recovered Mass, mg	Normalized Mass	J_s, Am^2/kg	χ_{lf}, 10^{-6} m^3/kg	λ, Earth, T^2/m	λ, Mars, T^2/m
Experiment HWMK8MA00, Wind Velocity Not Measured (Front), North of VLBA Road						
Base	280	---	0.91	8.17	1.51	0.57
Magnet 1	97.4	1.000	2.26	15.3	0.81	0.30
Magnet 2	38.4	0.394	2.23	16.7	0.74	0.28
Magnet 3	12.8	0.131	2.77	19.3	0.64	0.24
Magnet 4	9.3	0.095	1.26	17.4	0.71	0.27
Experiment HWMK8MA01, Wind Velocity Not Measured (Front), North of VLBA Road						
Base	240	---	0.68	6.73	1.83	0.69
Magnet 1	107.8	1.000	1.90	16.7	0.74	0.28
Magnet 2	21.1	0.196	3.49	24.5	0.50	0.19
Experiment HWMK9MA16, 0.0-3.0 m/s Wind (Front), West of Visitor's Center						
Base	471	---	1.07	12.3	1.00	0.38
Magnet 1	106.1	1.000	2.08	23.7	0.52	0.20
Magnet 2	50.8	0.479	3.08	29.5	0.42	0.16
Magnet 3	26.0	0.245	3.60	36.4	0.34	0.13
Magnet 4	24.2	0.228	2.93	30.1	0.41	0.15
Magnet 5	7.7	0.072	3.28	34.1	0.36	0.14
Experiment HWMK9MA19, 0.0-3.9 m/s Wind (Front), North VLBA Road						
Base	246	---	0.65	6.08	2.03	0.76
Magnet 1	96.2	1.000	1.02	7.88	1.56	0.59
Magnet 2	49.4	0.514	0.98	7.67	1.61	0.61
Magnet 3	24.0	0.249	1.01	7.78	1.58	0.60
Magnet 4	14.3	0.149	0.95	6.88	1.79	0.68
Magnet 5	5.6	0.058	0.80	6.77	1.82	0.69
Experiment HWMK9MA23, 1.6-8.0 m/s Wind (Front), South of VLBA Road						
Base	325	---	0.86	8.26	1.49	0.56
Magnet 1	54.2	1.000	2.41	18.3	0.67	0.25
Magnet 2	14.0	0.258	4.06	28.8	0.43	0.16
Magnet 3	6.0	0.111	3.39	25.0	0.49	0.19
Magnet 4	4.5	0.084	1.30	11.1	1.11	0.42
Experiment HWMK9MA24, 3.1-8.2 m/s Wind (Back), South of VLBA Road						
Base	483	---	0.85	8.07	1.53	0.58
Magnet 1	85.9	1.000	2.63	21.0	0.59	0.22
Magnet 2	10.2	0.119	7.79	56.7	0.22	0.08

[a]Normalized mass was calculated relative to mass collected on magnet 1. Dust samples collected form MA base are bulk dust.

suggest a bimodal distribution of particles with respect to magnetic properties for bulk palagonitic dust; (1) one mode is magnetic with $J_s \sim 2.5$ Am^2/kg (average J_s of collected dust; Table 5) and is collected by MA magnets, and (2) the other mode is less magnetic with $J_s \lesssim 0.31$ Am^2/kg (J_s of nonmagnetic separates; Table 4) and is not collected.

The mass collected from each magnet normalized to the mass collected from magnet 1 is plotted as a function of magnet strength in Figure 16c. Also plotted (dashed lines) are the relative capture cross sections [from *Madsen et al.*, 1999; Figure 7] corresponding to λ equal to 0.026 (maghemite), 0.3, 2.0, and 4.2 (hematite). With one exception the values of λ calculated for dust collected in our experiments fall between 0.3 and 2.0 (Table 5). Assuming that normalized collected mass is a surrogate for relative capture cross section, palagonitic dust collected in two experiments (HWMK8MA00 and HWMK9MA16) behaves as if it had magnetic properties similar to maghemite (i.e., $J_s \sim$ 50–74 Am^2/kg). We know that it is not the case by direct measurement ($J_s \sim$ 1-9 Am^2/kg; Figure 16a). A possible explanation is that the strongest magnet has approached or reached a steady state situation in which dust is being removed at the same rate that it is being collected while weaker magnets are still undergoing a net accumulation of dust. This situation would produce, as observed, a less steep dependence of normalized collected mass on magnet strength.

4.3. Summary

During MA experiments on Mauna Kea Volcano, palagonitic dust was collected by all five magnets when wind conditions permitted. Independent of wind conditions, we always observed collection of dust on at least three and usually four magnets after 16 min. The magnetic properties of collected dust varied from experiment to experiment, in response to variations in source material and environmental factors. The average values of J_s and χ_{lf} for palagonitic dust collected from the magnets were 2.5±1.5 Am^2/kg and (21±12)x10^{-6} m^3/kg, respectively. Both magnetic parameters are about a factor of 3 larger than the corresponding average values for bulk MA dust (0.84±0.15 Am^2/kg and

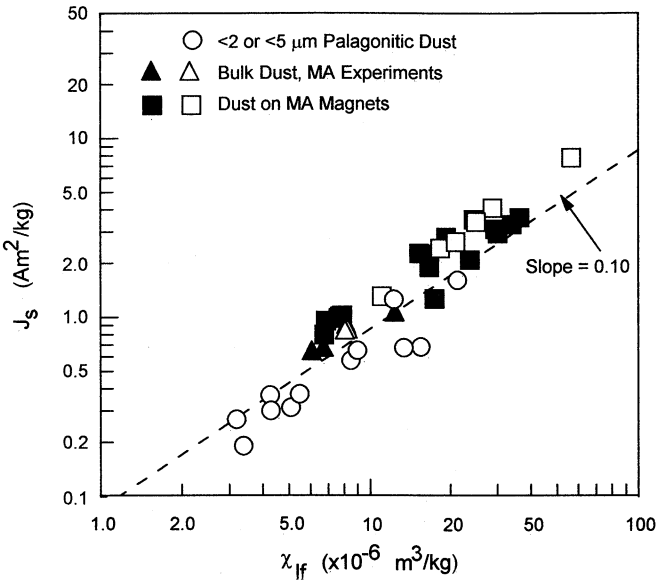

Figure 14. Saturation magnetization versus low-field magnetic susceptibility (293 K) for palagonitic dust obtained by size fractionation of bulk palagonitic tephra (circles) and palagonitic dust collected during MA experiments on Mauna Kea Volcano, Hawaii (squares and triangles). For MA data, solid and open symbols denote wind velocities less than and greater than 4 m/s, respectively.

$(8.3\pm2.2)x10^{-6}$ m^3/kg; calculated from Table 5), implying that a magnetic separation (culling of magnetic particles) occurred. Mössbauer spectra of collected dust showed that a multiphase assemblage was present, implying composite particles. Composite particles were observed directly in TEM photomicrographs of dust particles. The average relative collection efficiency of the magnets expressed as the mass collected by each magnet normalized to the mass collected by the strongest magnet is 100:33:18:14:6.5. The model of *Madsen et al.* [1999] underestimates the number of magnets that collect our palagonitic dust (three predicted and five observed) and underestimates the normalized collected mass as a function of magnet strength (dependence on magnet strength is weaker than predicted). At present, we have no satisfactory explanation for the difference between the model and our experimental observations.

5. Pathfinder Magnet Array Experiments on Mars

The results of the Pathfinder Magnet Array experiments are described in a series of papers [*Hviid et al.*, 1997; *Madsen et al.*, 1999; *Hargraves et al.*, 2000]. We first discuss their results relating to the magnetic properties of Martian dust (without regard to mineralogy and formation pathways) and the implications of our Mauna Kea simulation experiments for those results. We then consider mineralogical assignments and formation pathways.

5.1. Magnetic Properties

Martian dust was collected on the four strongest MA magnets by sol 68 [*Hviid et al.*, 1997; *Madsen et al.*, 1999]. Dust collection was detected on the strongest magnet first and, with increasing time, on progressively weaker magnets. The absence of dust on magnet 5, the results of the calculations of magnet capture cross sections, and the relative covering of the magnet suggests that discrete Martian dust particles are composite particles containing variable proportions of strongly magnetic phase and nonmagnetic or weakly magnetic phases and are characterized by a value of ~0.1 T^2/m for the λ parameter [*Madsen et al.*, 1999]. On the basis of results of simulation experiments with Mars analogue samples and comparison to calculated patterns where magnetic particles are potentially stable [*Madsen et al.*, 1999, Figure 10], the saturation magnetization of bulk Martian dust was estimated to be 4 ± 2 Am^2/kg. Their firm conclusion is that the dust is neither purely hematite (α-Fe_2O_3; J_s ~0.5 Am^2/kg) nor purely maghemite (γ-Fe_2O_3; J_s ~50-74 Am^2/kg) because those minerals would be collected by one or five magnets, respectively. The fact that some particles are collected by magnet 4 shows, according to *Madsen et al.* [1999], that a small fraction of the dust particles have J_s>10 Am^2/kg.

In support of their conclusion that Martian dust is composite particles having variable proportions of magnetic and nonmagnetic phases, *Madsen et al.* [1999] discuss a simulation experiment using thermally decomposed ocher (500°C, 24 hours) that has a bulk J_s of 7 Am^2/kg. They state that dust blown onto an MA under laboratory conditions sticks to the four strongest magnets (as on Mars). Material collected from magnets 2 and 4 have Mössbauer spectra characterized by more than one iron-bearing phase (one is

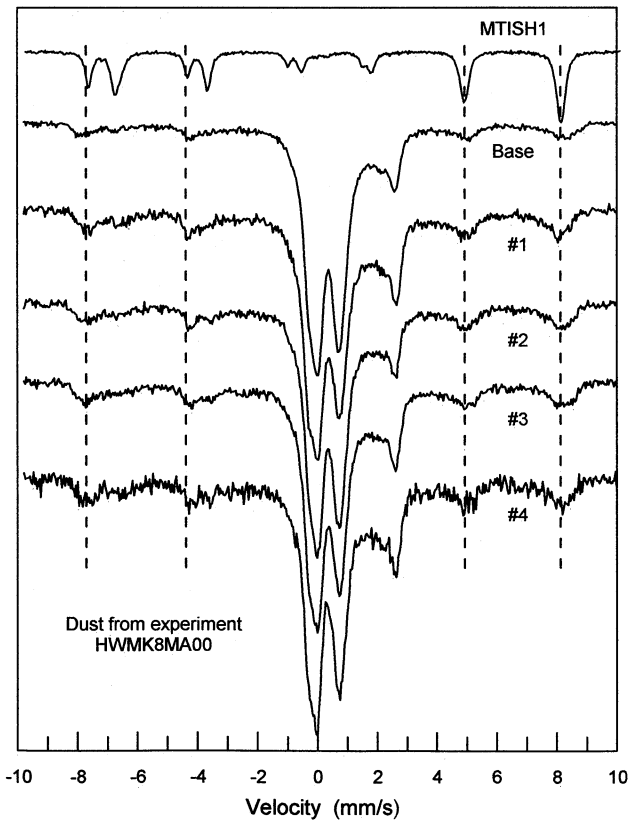

Figure 15. Mössbauer spectra (293 K) for palagonitic dust collected from the base of the MA and from magnets 1 through 4 for experiment HWMK8MA00. The Mössbauer spectrum for magnetite (MTISH1) is shown for reference. The *y* axis is in units of counts.

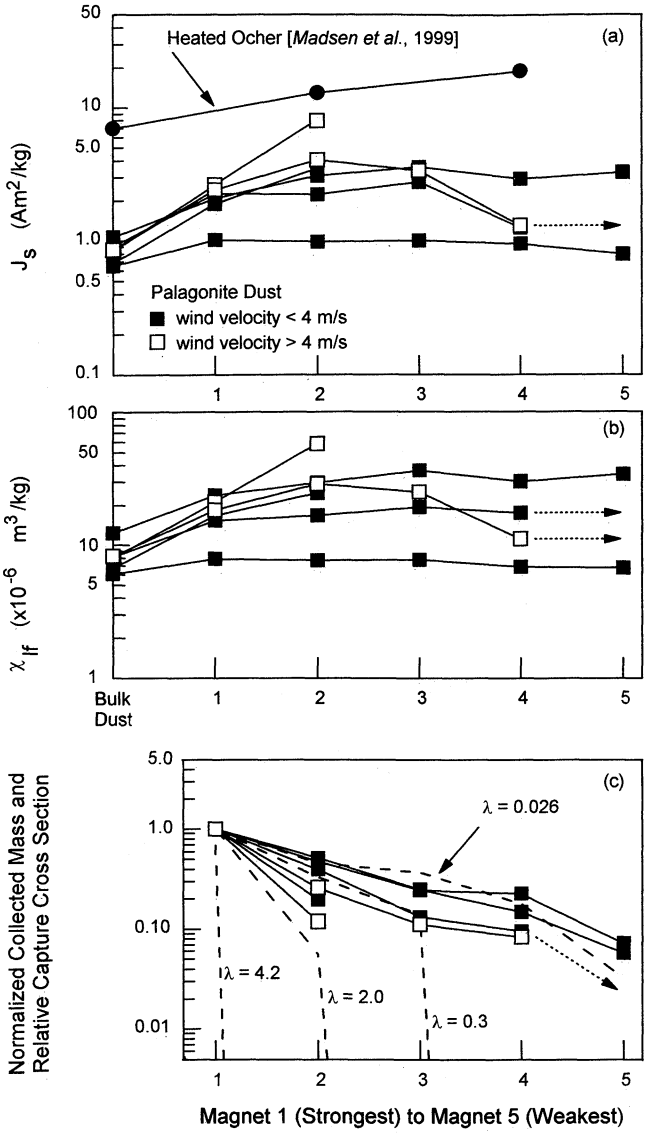

Figure 16. (a) Saturation magnetization, (b) low-field magnetic susceptibility, and (c) normalized collected mass as a function of Magnet Array magnet number. Also show in Figure 16c are the relative capture cross sections for four values of the λ parameter from *Madsen et al.* [1999].

maghemite) and have values of J_s equal to 13 and 19 Am²/kg, respectively [*Madsen et al.*, 1999]. These results are explained, according to *Madsen et al.* [1999], if the bulk decomposed ocher has composite particles that have variable proportions of magnetic and nonmagnetic phases and if the MA magnets sorted the composite particles according to their content of maghemite. They comment that, except for pure chemicals, sorting is normally observed. The measured value of J_s for the decomposed ocher from magnet 4 is >10 Am²/kg, in keeping with their inferred value of J_s for Martian dust on magnet 4.

Citing *Hargraves et al.* [1977] and *Pollack et al.* [1995] for the number density of 1-10 particles/cm³ for dust in the Martian atmosphere during the Viking mission, *Madsen et al.* [1999] use 1 particle/cm³ to calculate a rough estimate of the time for the strongest magnet to collect enough dust to see the target pattern. This time favorably compares with the time actually observed (~2 sol), so *Madsen et al.* [1999] conclude that a major fraction of the Martian atmospheric dust particles rather than a small subset are somewhat magnetic. Using the higher-density estimate (10 particles/cm³) reduces the fraction of dust particles that need to be sufficiently magnetic to be collected by the strongest magnet during the same time by an order of magnitude. During the Pathfinder mission, dust opacity and effective particle radius were about 0.5 and 1.7 μm, respectively [*Smith and Lemmon*, 1999], which gives a particle density of ~3 particles/cm³ [*Pollack et al.*, 1977, Equation (4)]. Thus, given the uncertainties on the number density of dust particles in the atmosphere, we consider that it is not actually possible to state whether a major fraction or a small subset of all dust particles are somewhat magnetic.

What are the implications of our Mauna Kea simulation experiments for the Mars Pathfinder experiment? One result is that palagonitic dust was collected by more magnets (all five) than was expected (three strongest magnets) on the basis of the *Madsen et al.* [1999] model and the independently measured magnetic properties of the palagonitic dust. This result implies that the 4±2 Am²/kg value of J_s estimated previously for Martian dust is too high [*Hviid et al.*, 1997; *Madsen et al.*, 1999]. If we base the interpretation of the Mars Pathfinder observations (dust on the four strongest magnets) on the Mauna Kea simulation experiments, the value of J_s for Martian dust is revised downward to 2.5±1.5 Am²/kg, which within the stated error is not significantly different from the *Madsen et al.* [1999] value. Our estimate may also be too high because it pertains to collection by five magnets and because the experiments were done in the gravity field of the Earth. In the model of *Madsen et al.* [1999], lower gravity results in lower values of the λ parameter, which increases the relative capture cross section [*Madsen et al.*, 1999, Figure 7]. The values of the λ parameter are given in Table 5 for both the Earth and Mars.

In the Mauna Kea experiments, the particle-to-particle variation in the magnetic properties of the collected (not bulk) dust was apparently too small to allow the observation of the magnetic sorting effect reported by *Madsen et al* [1999] for the thermally decomposed ocher, and the same is possible for Martian dust. As indicated by the difference in the values of J_s for palagonitic dust collected from the magnets (2.5±1.5 Am²/kg) and bulk dust (0.84±0.15 Am²/kg), a significant culling of magnetic particles occurred during the Mauna Kea experiments. To calculate the percentage of particles collected in Mauna Kea experiments, we must assume a value for the J_s of uncollected particles. Using values of J_s equal to 0 and 0.3 Am²/kg for uncollected dust particles gives 34 and 25 wt %, respectively, for the amount of bulk dust that was sufficiently magnetic to be collected by the MA magnets. To us these percentages, being <50 wt %, do not constitute a major portion of bulk dust. Whether they constitute a small subset or not is a matter of semantics. As discussed above, the fraction of dust particles on Mars that are sufficiently magnetic to be collected by the magnets is not well constrained because of the uncertainty in the number density of particles in the Martian atmosphere.

Our results are in agreement with the result of the Pathfinder Magnet Array Experiment [*Hviid et al.*, 1997; *Madsen et al.*, 1999; *Hargraves et al.*, 2000] and also the Viking Magnetic Properties Experiment [*Hargraves et al.*, 1977, 1979] that Martian dust contains at least one strongly magnetic mineral that is present as a component in composite

particles rather than as discrete magnetic particles. Our downward revision of J_s for Martian dust simply lowers the abundance of the strongly magnetic phase.

5.2. Maghemite Model

The preferred mineralogical assignment of *Hargraves et al.* [1979, 2000], *Hviid et al.* [1997], and *Madsen et al.* [1999] for the strongly magnetic component in Martian dust (and soil) is maghemite (γ-Fe_2O_3), which is present as the magnetic component of composite particles that are otherwise composed of nonmagnetic or weakly magnetic phases. The occurrence as a component of composite particles is based on their magnetic constraints and the result that Pathfinder soil, whose elemental composition they take (on the average) to be the same as that for aeolian dust, is basically silicate (not oxide) material [*Rieder et al.*, 1997]. In their view the maghemite is a fine-grained (perhaps <10 nm particles) material that precipitated as a stain or cement (i.e., a secondary mineral), yielding composite particles following oxidative chemical weathering of ferrous iron in silicate rocks. This process accommodates the small size of Martian dust particles (~3.4 μm diameter [*Markiewicz et al.*, 1999]), and, if the particle density in the Martian atmosphere is ~1 particle/cm^3, also provides a way to have the major portion of dust particles be somewhat magnetic and to have the content of maghemite vary from particle to particle.

Using J_s for pure maghemite (50-74 Am^2/kg) and the higher estimate of J_s for Martian dust (4±2 Am^2/kg), the maghemite content of the dust is 3-12 wt % as extreme limits and 6 wt % using nominal values of 4 and 70 Am^2/kg for the J_s of dust and maghemite, respectively. Assuming Martian dust has the same elemental composition as soil, all estimates of maghemite concentration are permitted within the constraint of the total Fe_2O_3 concentration measured for Martian soil (~18 wt % [*Rieder et al.*, 1997]). As most fully discussed by *Hargraves et al.* [2000], the Martian dust and soil is thus magnetically enhanced during soil formation relative to Martian surface rocks if the average magnetic properties of SNC meteorites (J_s=0.05-0.4 Am^2/kg) and/or the Martian equivalent of terrestrial ocean floor basalts (J_s~1.2 Am^2/kg) are representative of the average magnetic properties of Martian surface rocks.

In this model, maghemite as a cement or pigment contributes to the spectral properties of the aeolian dust at visible and near-IR wavelengths ("reddish appearance" [*Hargraves et al.*, 2000]). *Bell et al.* [2000] and *Madsen et al.* [1999] published multispectral data from the Imager for Mars Pathfinder (IMP) for dust collected by the strongest magnet on the upper and lower MAs. According to *Madsen et al.* [1999], a diffuse-reflectance approximation of a two-layer system was used for analysis of observed dust spectra to include consideration for an optically thin dust layer, and the spectra represent the reflectivity relative to that for the Pt-covered substrate. These spectra have the same general shape and both have reflectivity at 445 nm equal to 0.030. Subsequently, *Hviid et al.* [2000] published an IMP spectrum for dust collected by the strongest magnet of the lower MA that does not include considerations for optically thin dust. This spectrum has the same general shape as the previously published spectra, except that the reflectivity at 445 nm is ~0.37.

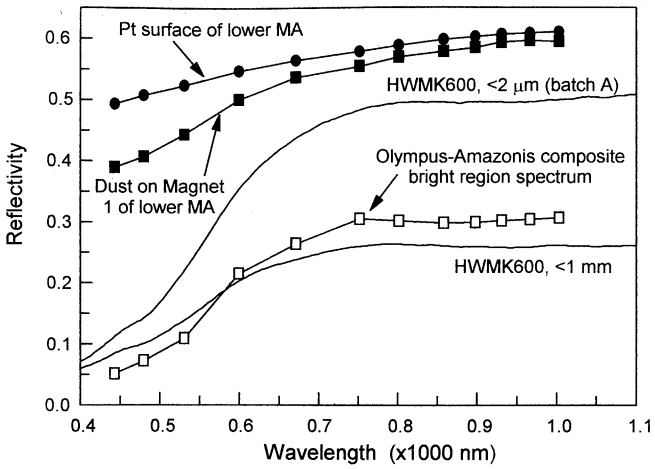

Figure 17. IMP reflectivity spectrum for Martian dust collected by the strongest magnet of the lower MA on Mars Pathfiner and a laboratory spectrum for the Pt-coated MA surface [*Hviid et al.*, 2000], laboratory spectra for bulk (<1 mm) palagonitic tephra HWMK600 and its palagonitic dust (<2 μm batch A) size separate [*Morris et al.*, 2000; this study], and the composite Olympus-Amazonis bright regions spectrum [*Mustard and Bell*, 1994] convolved to IMP band passes.

Figure 17 shows reflectivity data over the IMP multispectral range for the Pt metal surface of the lower MA (measured in the laboratory) and IMP spectra for dust on magnet 1 of the lower Pathfinder MA from *Hviid et al.* [2000], laboratory spectra for the <1 mm and <2 μm (batch A) size fractions of palagonitic spectra HWMK600 from this study and *Morris et al.* [2000], and the composite bright regions spectrum for the Olympus-Amazonis region from *Mustard and Bell* [1994]. As discussed by *Hviid et al.* [2000] and *Gunnlaugsson* [2000], the relationship of the spectra for the bare MA Pt-covered surface, the collected dust, and Martian bright regions implies that the dust collected by the magnet is not optically thick. Calculations were used in both papers to derive a "pure dust" spectrum. In the case of *Hviid et al.* [2000] the pure dust spectrum was obtained by using an empirical formula to fit the observed dust spectrum to the Olympus-Amazonis bright region spectrum at 440 and 670 nm. The fit is reasonably good, although the shallow band minimum near 850 nm in the Olympus-Amazonis spectrum is not reproduced in the MA dust spectrum. In the case of *Gunnlaugsson* [2000] the calculation involves setting the reflectivity at 440 nm for the pure dust spectrum equal to 0.03. Because of the different procedures used, the pure dust spectra published by *Hviid et al.* [2000] and *Gunnlaugsson* [2000] are somewhat different, but the general shapes are the same and none show evidence for a ferric band minimum in the region between 850 and 1000 nm.

The conclusion of *Hviid et al.* [2000] is that the spectral similarity of their pure magnetic dust and the Olympus-Amazonis bright regions implies that the magnetic dust is likely representative of Martian soil that is blown around the planet by the wind. Is this the case?

We indicated above that the Olympus-Amazonis spectrum has a shallow band minimum near 850 nm. As discussed previously [*Morris et al.*, 1989, 1997, 2000], this feature and

the relative reflectivity maximum near 750 nm are consistent with a disordered ferric-bearing material spectrally equivalent to np-Ox in palagonitic tephra plus subordinate (<5 wt %) red hematite. Other bright regions are characterized by a minimum near 900 nm [*Geissler et al.*, 1993; *Murchie et al.*, 1993], where, instead of red hematite, the subordinate component might be any combination of goethite, lepidocrocite, jarosite, schwertmannite, or maghemite [*Murchie et al.*,1993; *Bishop and Murad*, 1996; *Morris et al.*, 1996]. In contrast, the MA dust spectrum has no detectable minimum in the region between 800 and 1000 nm, so that the presence of a specific ferric oxide (including maghemite) cannot be inferred. In fact, the MA dust exhibits the smoothest and flattest 800-1000 nm spectral shape of all the soil and dust units defined by *Bell et al.* [2000]. Thus, although there is possible evidence for maghemite as a spectral component in some areas of the Martian surface that do not include the Pathfinder site, it is not ubiquitously present on the basis of spectral data. Spectral data, however, do not preclude the presence of maghemite in regions like Olympus-Amazonis because it is possible to spectrally mask maghemite with hematite and still satisfy the constraints of the Pathfinder magnetic properties experiment [*Morris et al.*, 1998a].

A possible explanation for the spectral observations is a two-component assemblage, where one component is blown by the wind, is magnetic, and has no band minimum between 800 and 1000 nm and the other component is relatively immobile surface materials that have a ferric band minimum whose position varies from place to place in bright regions on the planet.

In summary, the maghemite model is generally consistent with both magnetic and other data for the Martian surface. Although we believe that certain aspects of the model are not as robust as advocated [*Hargraves et al.*, 1979, 2000; *Hviid et al.*, 1997; *Madsen et al.*, 1999], including the fraction of dust particles that are somewhat magnetic and the role of maghemite as a pigment, it is a possible explanation for the magnetic component in Martian soil and dust. We would, however, revise the estimates of maghemite abundance downward by a factor ~2 because our estimate for the J_s of Martian dust, based on Mauna Kea simulation experiments, is a factor ~2 lower (2.5±1.5 Am^2/kg compared to 4±2 Am^2/kg). The revision gives 1.4-8 wt % as extreme limits for maghemite abundance and 4 wt % abundance using 2.5 and 70 Am^2/kg for the J_s of dust and maghemite, respectively.

To us a major shortcoming of the maghemite model is the absence of evidence that maghemite can actually form by dissolution of Fe^{2+} from silicate and perhaps oxide phases, oxidation of Fe^{2+} to Fe^{3+}, and chemical precipitation of maghemite [*Hargraves et al.*, 1979, 2000; *Hviid et al.*, 1997; *Madsen et al.*, 1999]. We are not aware of examples from the terrestrial literature where it can be unequivocally shown that maghemite forms as a direct precipitation product. According to *Cornell and Schwertmann* [1996], maghemite forms in terrestrial soils in two ways. The first way is aerial oxidation of lithogenic magnetite/titanomagnetite. Titanomaghemite formed in this manner is common in Brazilian soils developed from basaltic rocks [e.g., *Curi and Franzmeier*, 1987; *Allan et al.*, 1988, 1989; *Fontes and Weed,* 1991]. The formation of maghemite from virtually chemically pure magnetite by mild heating depends on the water content and possibly the size of the initial magnetite particles. Synthetic, fine-grained magnetite (aqueous synthesis) oxidizes to maghemite at low temperatures, a prerequisite for which may be some water (or OH) in the magnetite precursor [*Johnson and Merrill*, 1972, 1974; *Sidhu et al.,* 1981]. *Murad and Schwertmann* [1993] show that the oxidation of synthetic magnetite to maghemite occurs slowly even at room temperature. *Johnson and Merrill* [1972] show that the low-temperature oxidation products of two natural magnetite powders (presumably lithogenic) having minimum and intermediate particle diameters of <45 and <8 μm are hematite and hematite plus maghemite, respectively.

The second pathway for maghemite formation involves secondary minerals. Lepidocrocite (γ-FeOOH) undergoes thermal dehydroxylation to maghemite, but maghemite-rich soils on the Earth are not considered to have lepidocrocite precursors [*Cornell and Schwertmann*, 1996]. Goethite (α-FeOOH) and ferrihydrite ($Fe_2O_3 \cdot 9/5H_2O$) can be converted to maghemite in the presence of organic matter, if the organic matter does not oxidize before dehydroxylation of the oxides [e.g., *Cornell and Schwertmann*, 1996; *Campbell et al.*, 1997], to permit formation of fine-grained magnetite as an intermediate product. Possibly, maghemite formed by this process in the thermally altered ocher used as a Martian magnetic analogue by *Madsen et al.* [1999]. Maghemite in tropical and subtropical regions is associated with fires burning in vegetated soil [e.g., *Cornell and Schwertmann*, 1996].

Thus the terrestrial evidence is that maghemite does not form directly as a secondary mineral by precipitation from solution as advocated by *Hargraves et al.* [1979, 2000], *Hviid et al.* [1997], and *Madsen et al.* [1999]. A precursor (e.g., magnetite or lepidocrocite) seems to be a prerequisite for its formation. If it can be demonstrated that maghemite forms on Mars by direct precipitation as a result of chemical weathering, this formation pathway is common on the planet and so far unknown in terrestrial weathering environments.

With the probable exception of vegetative fires, all the other maghemite-forming processes discussed could produce the phase on Mars, and all have been previously suggested [*Coey et al.*, 1990; *Morris et al.*, 1990, 1997; *Banin et al.,* 1993; *Torrent and Barron*, 2001]. It is difficult to evaluate the lepidocrocite pathway (i.e., specific evidence for lepidocrocite), because its polymorph goethite (α-FeOOH) has the same chemical composition and similar magnetic and spectral properties. However, poorly crystalline lepidocrocite (and poorly crystalline goethite) cannot be excluded on the basis of Martian spectral data [*Bell et al.,* 2000; *Morris et al.*, 2000].

5.3. Magnetite/Titanomagnetite Model

In this model the strongly magnetic phase in Martian dust and soil is magnetite/titanomagnetite, whose origin is crystallization from silicate liquids or devitrification of silicate glass. Fe-Ti spinels formed in this way have been called "pyrogenetic" by *Hargraves et al.* [2000] and "lithogenic" by us [*Morris et al.*, 2000]. We include in this model silicate liquids (glasses) generated by any method, including igneous and impact processes.

Hargraves et al. [2000] argue against lithogenic (pyrogenetic) magnetite/titanomagnetite as the strongly magnetic phase in Martian dust and soil on the basis that titanomagnetite-containing materials on Mars are not

sufficiently magnetic (too low J_s) to account for the magnetic properties of soil and dust. In their discussion the following three kinds of titanomagnetite-containing materials and their associated values of J_s were considered: (1) Martian bedrock as represented by the SNC meteorites ($J_s \leq 0.5$ Am^2/kg); (2) Martian bedrock whose titanomagnetite composition and concentration are constrained by the composition of terrestrial ocean floor basalts ($Fe_{(3-x)}Ti_xO_4$, x=0.60) and the concentration of TiO_2 in Martian soil ($J_s \sim 1.2$ Am^2/kg); and (3) Martian surface material represented by palagonitic tephra ($J_s \sim 1$ Am^2/kg). The J_s for Martian dust used by *Hargraves et al.* [2000] (4±2 Am^2/kg) is significantly larger than all values of J_s listed above (0.5-1.2 Am^2/kg). Our downward revision of J_s for Martian dust (2.5±1.5 Am^2/kg) is still significantly larger than the J_s for SNC meteorites but is just within error of the values for ocean floor basalts and palagonitic tephra, suggesting that Martian basalts of similar composition and palagonitic tephra are possible within magnetic constraints. We discuss next additional reasons the arguments of *Hargraves et al.* [2000] do not exclude magnetite and/or titanomagnetite as the strongly magnetic phase in Martian dust.

Both estimates of the J_s for Martian bedrock by *Hargraves et al.* [2000] may be too low simply because they are based on SNC meteorites and terrestrial samples that are not fully representative of Martian surface rocks. The spectral similarity of Martian dark regions to SNC meteorites is evidence that SNCs are representative of surface rocks with respect to pyroxene mineralogy [*Singer and McSween*, 1993; *Mustard and Sunshine*, 1995; *Mustard et al.*, 1997], but the spectral analyses are not sensitive to variations in the abundance of relatively spectrally neutral minerals like magnetite. The discovery of linear magnetic anomalies on Mars [*Acuña et al.*, 1999; *Connerney et al.*, 1999] is possible evidence for rocks with high concentrations of (single domain) magnetite and/or titanomagnetite. Analyses of orbital spectra from the Mars Global Surveyor Thermal Emission Spectrometer instrument [*Bandfield et al.*, 2000] and APXS rock observations from the Pathfinder landing site [*Rieder et al.*, 1997; *McSween et al.*, 1999] also indicate the presence of compositions which are not represented by SNC meteorites.

Our Mauna Kea simulation experiments are direct experimental evidence that palagonitic tephra with Ti-bearing magnetite as the strongly magnetic phase in composite particles and bulk $J_s \sim 1$ Am^2/kg can satisfy the constraints of the Pathfinder MA experiment. It is also possible that glassy tephra on Mars is produced with higher concentrations of magnetite and/or titanomagnetite particles, which result in higher J_s values. Relative to unaltered glassy tephra, palagonitic tephra is not magnetically enhanced [*Morris et al.*, 2000], which is expected because the titanomagnetite particles are lithogenic (derived from the silicate liquid or glass) and not alteration products formed during glass palagonitization.

As suggested by *Morris et al.* [2000], impacts into Martian soil that produce impact melt in an oxidizing atmosphere might be an important source of basaltic glass with embedded magnetite/titanomagnetite particles. Like its volcanic counterpart, impact basaltic glass would be susceptible to alteration to palagonitic material. Terrestrial evidence for this process comes from titanomagnetite-containing basaltic glass formed at Lonar Crater, India [*Kieffer et al.*, 1976].

If we interpret the J_s of Martian dust to result entirely from magnetite, the average magnetite concentration of dust is ~(2.5)(100)/92 = 2.7 wt %. Chemically, this corresponds to 2.7x1.034 = 2.8 wt % Fe_2O_3. Using 19.7 wt % as the total chemical concentration of Fe_2O_3 in rock-free Martian soil (*Rieder et al.* [1997] as modified by *Morris et al.* [2000]), most of the iron in Martian dust (16.9 wt % calculated as Fe_2O_3) must be distributed among weakly magnetic and/or nonmagnetic iron-bearing phases (e.g., olivine, pyroxene, ilmenite, and nonmagnetic nanophase ferric oxides). Incorporation of Ti into the spinel increases the amount of the phase required to attain the J_s for Martian dust because incorporation of Ti lowers the J_s from that for pure magnetite [e.g., *Nagata,* 1961].

If magnetic material is contributed to Martian soil solely by the palagonitization of spinel-bearing impact melt glass, we would expect not every soil particle to be magnetic because fresh (nonmagnetic) material is introduced from some depth through regolith gardening by meteorites. Over time, however, the average amount of magnetic material in the soil would increase, so that the soil would become increasingly magnetically enhanced relative to the initial surface material. The implication for the Pathfinder MA experiments is that, analogous to our Mauna Kea experiments, culling of composite magnetic particles from the dust would likely take place. As discussed above, we believe that available data do not constrain the extent of culling during the Pathfinder MA experiments.

5.4. Summary

Palagonitic dust from Mauna Kea Volcano contains a subset of composite dust particles that is sufficiently magnetic to be collected by all five Pathfinder MA magnets. The average J_s of this dust is 2.5±1.5 Am^2/kg, and we use this average as a downward revision of the J_s previously inferred for magnetic Martian dust (4±2 Am^2/kg) by *Hviid et al.* [1997], *Madsen et al.* [1999], and *Hargraves et al.* [2000]. This revision depends only on the magnetic properties of the collected dust and is independent of its mineralogical composition.

The Pathfinder MA experiment is consistent with a model in which Martian dust is the end product of palagonitization of glassy materials that contains magnetite/titanomagnetite particles (as the strongly magnetic phase) and other silicate phases (e.g., plagioclase and pyroxene) in an oxidizing environment. The glassy material originates from volcanic and/or impact processes [*Morris et al.*, 2000]. This model accounts for both the spectral and magnetic properties of Martian dust and soil. We observed culling of magnetic particles from bulk palagonitic dust in the Mauna Kea experiments; it is uncertain whether culling occurs on Mars. If culling is not observed for Martian dust, the difference may represent a mineralogical difference in glassy precursor materials on Mauna Kea and on Mars, and, in either event, the J_s revision is valid. The impacting projectiles could also augment the population of composite magnetic soil and dust particles by dissemination of impactor magnetic minerals (metallic iron, maghemite, and magnetite) throughout target materials. If the magnetic minerals in Martian soil and dust are formed mostly in response to impact processes (impactor dissemination and spinel crystallization from impact melts), Martian soil and dust are magnetically enhanced relative to

Martian rocks. Magnetic enhancement is observed for the Moon, where the soil has an excess of metallic iron relative to the rocks from metallic iron in impactors and from reduction of ferrous iron to metal in the soil [e.g., *Housley et al.*, 1973; *Morris et al.*, 1998b]. Our model does not require, but does not exclude, maghemite produced by weathering of ferrous silicates as a contributory process to the formation of magnetic Martian soil [*Hviid et al.*, 1997; *Madsen et al.*, 1999; *Hargraves et al.*, 2000].

Acknowledgments. This work was supported by NASA's Cosmochemistry Program under RTOP 344-31-20-24 (R.V.M.) and NASA's Mars Data and Analysis Program under RTOP 896-50-72-01 (R.V.M.) and by NSF (award EAR-9217945) and Franklin and Marshall College (S.A.M.). S.A.M. thanks Karen R. Mertzman for her invaluable work in the sample preparation laboratory. E. Cloutis and V. Hamilton provided thoughtful and detailed reviews.

References

Acuña, M. H., et al., Global distribution of crustal magnetization discovered by the Mars Global Surveyor MAG/ER experiment, *Science, 284,* 790-793, 1999.

Allan, J. E. M., J. M. D. Coey, M. Resende, and J. D. Fabris, Magnetic properties of iron-rich oxisols, *Phys. Chem. Miner., 15,* 470-475, 1988.

Allan, J. E. M., J. M. D. Coey, I. S. Sanders, U. Schwertmann, G. Friedrich, and A. Wiechowski, An occurrence of a fully-oxidized natural titanomaghemite in basalt, *Min. Mag., 53,* 299-304, 1989.

Allen, C. C., J. L. Gooding, M. Jercinovic, and K. Keil, Altered basaltic glass: A terrestrial analog to the soil of Mars, *Icarus, 45,* 347-369, 1981.

Allen, C. C., K. M. Jager, R. V. Morris, D. J. Lindstrom, M. M. Lindstrom, and J. P. Lockwood, Martian soil simulant available for scientific, educational study, *Eos Trans. AGU, 79*(34), 405, 408-409, 1998.

Bandfield, J. L., V. E. Hamilton, and P. R. Christensen, A global view of martian surface compositions from MGS-TES, *Science, 287,* 1626-1630, 2000.

Banin, A., T. Ben-Shlomo, L. Margulies, D. F. Blake, R. L. Mancinelli, and A. U. Gehring, The nanophase iron mineral(s) in Mars soil, *J. Geophys. Res., 98,* 20,831-20,853, 1993.

Bates, R. L., and J. A. Jackson Ed., *Dictionary of Geological Terms,* 3rd ed., 571 pp., Doubleday, New York, 1984.

Bell, J. F., III, R. V. Morris, and J. B. Adams, Thermally altered palagonitic tephra: A spectral and process analog to the soil and dust of Mars, *J. Geophys. Res., 98,* 3373-3385, 1993.

Bell, J. F., III, et al., Mineralogic and compositional properties of Martian soil and dust: Results from Mars Pathfinder, *J. Geophys. Res., 105,* 1721-1755, 2000.

Bishop, J. L., and E. Murad, Schwertmannite on Mars? Spectroscopic analyses of schwertmannite, its relationship to other ferric minerals, and its possible presence in the surface material on Mars. *Mineral Spectroscopy: A Tribute to Roger G. Burns,* edited by M. D. Dyar, C. McCammon, and M. W. Schaefer, Spec. Publ. Geochem. Soc., 5, 337-358, 1996.

Bishop, J. L., and C. M. Pieters, Low-temperature and low atmospheric pressure infrared reflectance spectroscopy of Mars soil analog materials, *J. Geophys. Res., 100,* 5369-5379, 1995.

Bishop, J. L., C. M. Pieters, and J. O. Edwards, Infrared spectroscopic analyses on the nature of water in montmorillonite, *Clays Clay Miner., 42,* 702-716, 1994.

Boyd, F. R., and S. A. Mertzman, Composition and structure of the Kaapvaal lithosphere, southern Africa, *Magmatic Processes - Physicochemical Principles, edited by* B. O. Mysen, Spec. Publ. Geochem. Soc., 1, 13-24, 1987.

Brady, P. V., R. I. Dorn, A. J. Brazel, J. Clark, R. B. Moore, and T. Glidewell, Direct measurement of the combined effects of lichen, rainfall, and temperature on silicate weathering, *Geochim. Cosmochim. Acta, 63,* 3293-3300, 1999.

Campbell, A. S., U. Schwertmann, and P. A. Campbell, Formation of cubic phases on heating ferrihydrite, *Clay Miner., 32,* 615-622, 1997.

Clark, R. N., G. A. Swayze, R. B. Singer, and J. B. Pollack, High-resolution reflectance spectra of Mars in the 2.3-μm region: Evidence for the mineral scapolite, *J. Geophys. Res., 95,* 14,463-14,480, 1990.

Coey, J. M. D., S. Morup, M. B. Madsen, and J. M. Knudsen, Titanomaghemite in magnetic soils on Earth and Mars, *J. Geophys. Res., 95,* 14,423-14,425, 1990.

Connerney, J. E. P., M. H. Acuna, P. J. Wasilewski, N. F. Ness, H. Reme, C. Mazelle, D. Vignes, R. P. Lin, D. L. Mitchell, and P. A. Cloutier, Magnetic lineations in the ancient crust of Mars, *Science, 284,* 794-798, 1999.

Cooper, C. D., and J. F. Mustard, Effects of very fine particle size on reflectance spectra of smectite and palagonitic soil, *Icarus, 142,* 557-570, 1999.

Cornell, R., and U. Schwertmann, *The Iron Oxides: Structure, Properties, Reactions, Occurrences, and Uses*, 573 pp., John Wiley, New York, 1996.

Curi, N., and D. P. Franzmeier, Effect of parent rocks on chemical and mineralogical properties of some oxisols in Brazil, *Soil Sci. Soc. Am. J., 51,* 153-158, 1987.

Eggleton, R., Noncrystalline Fe-Si-Al-oxyhydroxides, *Clays Clay Miner., 35,* 29-37, 1987.

Eggleton, R. A., and J. Keller, The palagonitization of limbergite glass, *Neues. Jahrb. Minerol. Monatsh. Jg., H7,* 321-336, 1982.

Eggleton, R. A., and D. B. Tilley, Hisingerite: A ferric kaolin mineral with curved morphology, *Clays Clay Miner., 46,* 400-413, 1998.

Farmer, V. C., Possible confusion between so-called ferrihydrites and hisingerites, *Clay Miner., 27,* 373-378, 1992.

Fontes, M. P. F., and S. B. Weed, Iron oxides in selected Brazilian oxisols, I, Mineralogy, *Soil Sci. Soc. Am. J., 55,* 1143-1149, 1991.

Geissler, P. E., R. B. Singer, G. Komatsu, S. Murchie, and J. Mustard, An unusual spectral unit in West Candor Chasma: Evidence for aqueous or hydrothermal alteration in the Martian canyons, *Icarus, 106,* 380-391, 1993.

Golden, D. C., R. V. Morris, H. V. Lauer Jr., and S. R. Yang, Mineralogy of three slightly palagonitized tephra samples from the summit of Mauna Kea, Hawaii, *J. Geophys. Res., 98,* 3401-3411, 1993.

Gunnlaugsson, H. P., Analysis of the Magnetic Properties Experiment data from Mars: Results from Mars Pathfinder, *Planet. Space. Sci., 48,* 1491-1504, 2000.

Gunnlaugsson, H. P., S. F. Hviid, J. M. Knudsen, and M. B. Madsen, Instruments for the magnetic properties experiments on Mars Pathfinder, *Planet. Space. Sci., 46,* 449-459, 1998.

Hargraves, R. B., D. W. Collinson, R. V. Arvidson, and C. R. Spitzer, The Viking magnetic properties experiment: Primary mission results, *J. Geophys. Res., 82,* 4547-4558, 1977.

Hargraves, R. B., D. W. Collinson, R. E. Arvidson, and P. M. Cates, Viking magnetic properties experiment: Extended mission results, *J. Geophys. Res., 84,* 8379-8384, 1979.

Hargraves, R. B., J. M. Knudsen, P. Bertlesen, W. Goetz, H. P. Gunnlaugsson, S. F. Hviid, M. B. Madsen, and M. Olsen, Magnetic enhancement on the surface of Mars?, *J. Geophys. Res., 105,* 1819-1827, 2000.

Henmi, T., K. Tange, T. Minagawa, and N. Yoshinaga, Effect of SiO_2/Al_2O_3 ratio on the thermal reactions of allophane, II, Infrared and X-ray powder diffraction data, *Clays Clay Miner., 29,* 124-128, 1981.

Housley, R. M., R. W. Grant, and N. E. Paton, Origin and characteristics of excess Fe metal in lunar glass welded aggregates, *Proc. Lunar Sci. Conf. 4th,* 2373-2749, 1973.

Hunt, G. R., and J. W. Salisbury, Visible and near-infrared spectra of minerals and rocks, I, Silicate minerals, *Mod. Geol., 1,* 283-300, 1970.

Hviid, S. F., et al., Magnetic properties experiments on the Mars Pathfinder Lander: Preliminary results, *Science, 278,* 1768-1770, 1997.

Hviid, S. F., J. M. Knudsen, M. B. Madsen, and R. B. Hargraves, Spectroscopic investigation of the dust attracted to the magnetic properties experiment on the Mars Pathfinder lander, *Lunar Planet. Sci. XXXI* [CD-ROM], abstract 1641, 2000.

Jackson, M. L., *Soil Chemical Analysis--Advanced Course*, 895 pp., published by the author, Madison, Wis., 1985.

Jeong, G., J., The dependence of localized crystallization of halloysite and kaolinite on primary minerals in the weathering profile of granite, *Clays Clay Miner., 48,* 196-203, 2000.

Johnson, H. P., and R. T. Merrill, Magnetic and mineralogical changes associated with low-temperature oxidation of magnetite, *J. Geophys. Res., 77,* 334-341, 1972.

Johnson, H. P., and R. T. Merrill, Low-temperature oxidation of a titanomagnetite and the implications for paleomagnetism, *J. Geophys. Res., 78,* 4938-4949, 1973.

Johnson, H. P., and R. T. Merrill, Low-temperature oxidation of a single-domain magnetite, *J. Geophys. Res., 79,* 5533-5534, 1974.

Johnston, C. T., G. Sposito, and C. Ericsson, Vibrational probe studies of water interaction with montmorillonite, *Clays Clay Miner., 40,* 722-730, 1992.

Kawano, M., K. Tomita, and Y. Shinohara, Analytical electron microscopic study of the noncrystalline products formed at early weathering stages of volcanic glass, *Clays Clay Miner., 45,* 440-447, 1997.

Kerridge, J. F., Some observations on the nature of magnetite in the Orgueil meteorite, *Earth Planet. Sci. Lett., 9,* 299-306, 1970.

Kerridge, J. F., A. L. Mackay, and W. V. Boynton, Magnetite in CI carbonaceous meteorites: Origin by aqueous activity on a planetesimal surface, *Science, 205,* 395-397, 1979.

Kieffer, S. W., R. B. Schaal, R. Gibbons, F. Horz, D. J. Milton, and A. Dube, Shocked basalt from Lonar Impact Crater, India, and experimental analogues, *Proc. Lunar Sci. Conf. 7th,* 1391-1412, 1976.

Madsen, M. B., S. F. Hviid, H. P. Gunnlaugsson, J. M. Knudsen, W. Goetz, C. T. Pedersen, A. R. Dinesen, C. T. Morgensen, M. Olsen, and R. B. Hargraves, The magnetic properties experiments on Mars Pathfinder, *J. Geophys. Res., 104,* 8761-8779, 1999.

Markiewicz, W. J., R. M. Sablotny, H. U. Keller, N. Thomas, D. Titov, and P. Smith, Optical properties of the Martian aerosols derived from Imager for Mars Pathfinder midday sky brightness data, *J. Geophys. Res., 104,* 9009-9017, 1999.

McSween, H.Y., Jr., et al., Chemical, multispectral, and textural constraints on the composition and origin of rocks at the Mars Pathfinder landing site, *J. Geophys. Res., 104,* 8679-8716, 1999.

Moro, M. C., M. L. Cembranos, and A. Fernandez, Allophane-like materials in the weathered zones of Silurian phosphate-rich veins from Santa Creu d'Olorda (Barcelona, Spain), *Clay Miner., 35,* 411-421, 2000.

Morris, R. V., and D. C. Golden, Goldenrod pigments and the occurrence of hematite and possibly goethite in the Olympus-Amazonis region of Mars, *Icarus, 134,* 1-10, 1998.

Morris, R. V., H. V. Lauer Jr., C. A. Lawson, E. K. Gibson Jr., G. A. Nace, and C. Stewart, Spectral and other physicochemical properties of submicron powders of hematite (α-Fe_2O_3), maghemite (γ-Fe_2O_3), magnetite (Fe_3O_4), goethite (α-FeOOH), and lepidocrocite (γ-FeOOH), *J. Geophys. Res., 90,* 3126-3144, 1985.

Morris, R. V., D. G. Agresti, H. V. Lauer Jr., J. A. Newcomb, T. D. Shelfer, and A. V. Murali, Evidence for pigmentary hematite on Mars based on optical, magnetic, and Mossbauer studies of superparamagnetic (nanocrystalline) hematite, *J. Geophys. Res., 94,* 2760-2778, 1989.

Morris, R. V., J. J. Gooding, H. V. Lauer Jr., and R. B. Singer, Origins of Marslike spectral and magnetic properties of a Hawaiian palagonitic soil, *J. Geophys. Res., 95,* 14,427-14,434, 1990.

Morris, R. V., H. V. Lauer Jr., D. G. Schulze, and R. G. Burns, Preparation and characterization of a nanophase hematite powder, *Lunar Planet. Sci. XXII,* The Lunar and Planetary Institute, Houston, 927-928, 1991.

Morris, R. V., D. C. Golden, J. F. Bell III, H. V. Lauer Jr., and J. B. Adams, Pigmenting agents in Martian soils: Inferences from spectral, Mossbauer, and magnetic properties of nanophase and other iron oxides in Hawaiian palagonitic soil PN-9, *Geochim. Cosmochim. Acta, 57,* 4597-4609, 1993.

Morris, R. V., D. W. Ming, D. C. Golden, and J. F. Bell III, An occurrence of jarositic tephra on Mauna Kea, Hawaii: Implications for the ferric mineralogy of the Martian surface. *Mineral Spectroscopy: A Tribute to Roger G. Burns,* edited by M. D. Dyar, C. McCammon, and M. W. Schaefer, Spec. Publ. Geochem. Soc., 5, 327-336, 1996.

Morris, R. V., D. C. Golden, and J. F. Bell III, Low-temperature reflectivity spectra of red hematite and the color of Mars, *J. Geophys. Res., 102,* 9125-9133, 1997.

Morris, R. V., D. C. Golden, T. D. Shelfer, and H. V. Lauer Jr., Lepidocrocite to maghemite to hematite: A pathway to magnetic and hematitic Martian soil, *Meteorit. Planet. Sci., 33,* 743-751, 1998a.

Morris, R. V., G. Klingelhofer, R. L. Korotev, and T. D. Shelfer, Mossbauer mineralogy on the Moon: The lunar regolith, *Hyperfine Interact., 117,* 405-432, 1998b.

Morris, R. V., et al., Mineralogy, composition, and alteration of Mars Pathfinder rocks and soils: Evidence from multispectral, elemental, and magnetic data on terrestrial analogue, SNC meteorite, and Pathfinder samples, *J. Geophys. Res., 105,* 1757-1817, 2000.

Moskowitz, B. M., and R. B. Hargraves, Magnetic changes accompanying the thermal decomposition of nontronite (in air) and its relevance to Martian mineralogy, *J. Geophys. Res., 87,* 10,115-10,128, 1982.

Murad, E., and U. Schwertmann, Temporal stability of fine-grained magnetite, *Clays Clay Miner., 41,* 111-113, 1993.

Murchie, S., J. Mustard, J. Bishop, J. Head, and C. Pieters, Spatial variations in the spectral properties of bright regions on Mars, *Icarus, 105,* 454-468, 1993.

Murphy, J. R., R. M. Haberle, O. B. Toon, and J. B. Pollack, Martian global dust storms: Zonally symmetric numerical simulations including size-dependent particle transport, *J. Geophys. Res., 98,* 3197-3220, 1993.

Mustard, J. F., and J. F. Bell III, New composite reflectance spectra of Mars from 0.4 to 3.14 μm, *Geophys. Res. Lett., 21,* 353-356, 1994.

Mustard, J. F., and J. M. Sunshine, Seeing through the dust: Martian crustal heterogeneity and links to the SNC meteorites, *Science, 267,* 1623-1626, 1995.

Mustard, J. F., S. Murchie, S. Erard, and J. Sunshine, In situ compositions of Martian volcanics: Implications for the mantle, *J. Geophys. Res., 102,* 25,605-25,615, 1997.

Nagata, T., *Rock Magnetism*, 350 pp., Maruzen, Tokyo, 1961.

Palmer, H. C., K. Tazaki, W. S. Fyfe, and Z. Zhou, Precambrian glass, *Geology, 16,* 221-224, 1988.

Parfitt, R. L., C. W. Childs, and D. N. Eden, Ferrihydrite and allophane in four andepts from Hawaii and implications for their classification, *Geoderma, 41,* 223-241, 1988.

Pollack, J. B., D. Colburn, R. Kahn, J. Hunter, W. van Camp, C. E. Carlston, and M. R. Wolf, Properties of aerosols in the Martian atmosphere, as inferred from Viking lander imaging data, *J. Geophys. Res., 82,* 4479-4496, 1977.

Pollack, J. B., M. E. Ockert-Bell, and M. K. Shepard, Viking lander image analysis of Martian atmospheric dust, *J. Geophys. Res, 100,* 5235-5250, 1995.

Reichen, L. E., and J. J. Fahey, An improved method for the determination of FeO in rocks and minerals including garnet, *U.S. Geol. Surv. Bull., 1144B,* 1-5, 1962.

Rieder, R., T. Economou, H. Wanke, A. Turkevich, J. Crisp, J. Bruckner, G. Drebus, and H. Y. McSween Jr., The chemical composition of Martian soil and rocks returned by the mobile alpha proton X-ray spectrometer: Preliminary results from the X-ray mode, *Science, 278,* 1771-1774, 1997.

Schiffman, P., H. J. Spero, R. J. Southard, and D. A. Swanson, Controls on palagonitization versus pedogenic weathering of basaltic tephra: Evidence from the consolidation and geochemistry of the Keanakako'i Ash Member, Kilauea Volcano, *Geochem. Geophys. Geosyst., 1,* Paper number 2000GC000068 [6594 words, 5 figures, 4 tables], 2000.

Sidhu, P. S., R. J. Glikes, and A. M. Posner, Oxidation and ejection of nickel and zinc from natural and synthetic magnetites, *Soil Sci. Soc. Am. J., 45,* 641-644, 1981.

Singer, R. B., Spectral evidence for the mineralogy of high-albedo soils and dust on Mars, *J. Geophys. Res., 87,* 10,159-10,168, 1982.

Singer, R. B., and H. Y. McSween Jr., The igneous crust of Mars: Compositional evidence from remote sensing and the SNC meteorites, *Resources of Near-Earth Space*, edited by J. S. Lewis, M. S. Matthews, and M. M. L. Guerrierim, pp. 709-736, Univ. of Ariz. Press, Tucson, 1993.

Smith, P. H., and M. Lemmon, Opacity of the Martian atmosphere measured by the Imager for Mars Pathfinder, *J. Geophys. Res., 104,* 8975-8985, 1999.

Smith, P. H., et al., Results from the Mars Pathfinder camera, *Science, 278,* 1558-1765, 1997.

Stacey, F. D., and S. K. Banerjee, *The Physical Principles of Rock Magnetism*, Elsevier Sci., New York, 1974.

Syers, J. K., M. L. Jackson, V. E. Berkheiser, R. N. Clayton, and R. W. Rex, Eolian sediment influence on pedogenesis during the quaternary, *Soil Sci., 107,* 421-427, 1969.

Tazaki, K., Observation of primitive clay precursors during microcline weathering, *Contrib. Mineral. Petrol., 92,* 86-88, 1986.

Tazaki, K., and W. S. Fyfe, Primitive clay precursors formed on feldspar, *Can. J. Earth Sci., 24,* 506-527, 1987.

Tazaki, K., W. S. Fyfe, and S. J. van der Gaast, Growth of clay minerals in natural and synthetic glasses, *Clays Clay Miner., 37,* 348-354, 1989.

Torrent, J., and V. Barron, Key role of phosphorus in the formation of the iron oxides in Mars soils?, *Icarus, 145,* 645-647, 2000.

Ugolini, F. C., Hydrothermal origin of the clays from the upper slopes of Mauna Kea, Hawaii, *Clays Clay Miner., 22,* 189-194, 1974.

Wada, S.-I., and C. Mizota, Iron-rich halloysite (10A) with crumpled lamellar morphology from Hokkaido, Japan, *Clays Clay Miner., 30,* 315-317, 1982.

Weidner, V. R., and J. J. Hsia, Reflection properties of pressed polytetrafluoroethylene powder, *J. Opt. Soc. Am., 71,* 856-861, 1981.

J. F. Bell III, Department of Astronomy, Cornell University, Ithaca, NY 44853.

D. C. Golden, Hernandez Engineering, Inc., Houston, TX 77058.

T. G. Graff and T. D. Shelfer, Lockheed Martin Space Operations Company, Houston, TX 77078.

L. C. Jørgensen, Niels Bohr Institute for Astronomy, Physics and Geophysics, Ørsted Laboratory, Universitetsparken 5, University of Copenhagen, DK 2100 Copenhagen Ø, Denmark.

S. A. Mertzman, Department of Geosciences, Franklin and Marshall College, Lancaster, PA 17604.

D. W. Ming and R. V. Morris, NASA Johnson Space Center, Houston, TX 77058. (richard.v.morris1@jsc.nasa.gov)

(Received July 14, 2000; revised November 29, 2000;
accepted January 5, 2001)